DOKUZ EYLÜL UNIVERSITY
IZMIR INTERNATIONAL
BIOMEDICINE AND GENOME
INSTITUTE

MODELLING NEUROENDOCRINE DIFFERENTIATION IN BLADDER CANCER AND ANALYSIS PHENOTYPIC AND MOLECULAR EFFECTS

EZGI BOYVATLI

MOLECULAR BIOLOGY AND GENETICS

MASTER'S THESIS İZMİR-2023

THESIS ID: DEU.IBG.MSc/2020850021

DOKUZ EYLÜL UNIVERSITY
IZMIR INTERNATIONAL
BIOMEDICINE AND GENOME
INSTITUTE

MODELLING NEUROENDOCRINE DIFFERENTIATION IN BLADDER CANCER AND ANALYSIS PHENOTYPIC AND MOLECULAR EFFECTS

EZGİ BOYVATLI

MOLECULAR BIOLOGY AND GENETICS

MASTER'S THESIS İZMİR-2023

ADVISOR: DOÇ.DR. ŞERİF ŞENTÜRK CO-ADVISOR: DOÇ.DR. SERAP ERKEK ÖZHAN

This study is supported by TÜBİTAK 2247

THESIS ID: DEU.IBG.MSc/2020850021

T.C.
DOKUZ EYLÜL ÜNİVERSİTESİ

İZMİR ULUSLARARASI BİYOTIP VE GENOM ENSTİTÜSÜ

YÜKSEK LİSANS TEZ SAVUNMA SINAVI TUTANAĞI

Dokuz Eylül Üniversitesi İzmir Uluslararası Biyotıp ve Genom Enstitüsü Moleküler Biyoteknoloji Anabilim Dalı, Moleküler Biyoloji ve Genetik Yüksek Lisans programı öğrencisi 2020850021 numaralı öğrencisi Ezgi BOYVATLI, "'Mesane Kanserinde Nöroendokrin Farklılaşmanın Modellenmesi ve Fenotipik ve Moleküler Etkilerinin Araştırılması." konulu Yüksek Lisans tezini 16.08.2023 tarihinde yapılan savunma sınavı sonucunda başarılı / ~~başarısız~~ olmuştur.

BAŞKAN
Doç. Dr. Şerif ŞENTÜRK

JÜRİ ÜYESİ
Doç. Dr. Duygu SAĞ

JÜRİ ÜYESİ
Prof. Dr. Özden YALÇIN ÖZUYSAL

TABLE OF CONTENT

TABLE OF CONTENT i

INDEX OF FIGURES iv

INDEX OF TABLES v

ABBREVIATIONS vi

ACKNOWLEDGEMENTS vii

ABSTRACT .....

1 ÖZET 2

1. INTRODUCTION AND AIM 3
2. GENERAL INFORMATION 4
    - 2.1. Bladder Cancer General Characteristics 4
        - 2.1.1. Molecular Characterization of Bladder Cancer 5
        - 2.1.2. Neuroendocrine Subtype of Bladder Cancer 7
    - 2.2. Role of β-catenin Dependent Wnt Pathway in Cancer 9
    - 2.3. Role of EGF Signaling in Cancers 11
    - 2.4. Modelling of Neuroendocrine Cancers 12
        - 2.4.1. Origin of Neuroendocrine Tumors 12
        - 2.4.2. Gene Editing/ Gene-Character Change Based Approaches 14
        - 2.4.3. Induction Based Methods 14
3. MATERIALS AND METHODS 16

3.1. Type of The Research 16
3.2. The Time and The Place of The Research 16
3.3. Research Materials 16
3.3.1. Laboratory Equipment and Supplies 17
3.3.2. Commercial Kits 18
3.3.3. Cell Culture 19
3.3.4. General Chemical 20
3.3.5. Western Blots Buffers 21
3.3.6. Plasmids used for WNT Reporter Assay 23
3.3.7. Bacteria 23
3.3.8. Antibodies 24
3.3.9. qRT-PCR primers 25
3.3.10. Genome Editing 25
3.4. Experiments..... 28
3.4.1. Cell lines and cell culture 28
3.4.2. Induction Based Neuroendocrine Differentiation 28
3.4.2.1. EGF Treatment 28

3.4.2.2. RNA and protein isolation 29
3.4.2.3. cDNA conversion 29
3.4.2.4. IF staining 29
3.4.2.5. BCA Assay and WB..... 30
3.4.2.6. qRT-PCR 32
3.4.2.7. WNT reporter assay..... 32
3.4.2.8. MTT assay 33
3.4.2.9. Colony formation assay 33
3.4.2.10. Wound healing assay..... 33
3.4.2.11. Spheroid formation assay 34
3.4.2.12. Cell cycle assay 34
3.4.3. Gene Editing Based Neuroendocrine Differentiation 35
3.4.3.1. CRISPR-Cas9 HDR 35
3.4.3.1.1. Oligo Design 35
3.4.3.1.2. sgRNA Synthesis 35

3.4.3.1.3. T7 In Vitro Transcription 35
3.4.3.1.4. RNA purification 36
3.4.3.1.5. In Vitro Cas9 Cleavage Assay 36
3.4.3.2. Overexpression of Mutated Genes 36
3.4.3.2.1. Generation of Plasmid Stocks Obtained from Addgene 36
3.4.3.2.2. Generation of CTNNB1-S45F, KRAS G12D and ARID1A W2050* Plasmids and Preparation for Lentiviral Transduction 37
3.4.3.2.3. Lentiviral Transduction for PHAGE-KRAS-G12D Plasmid 39
3.5. Data evaluation 40
3.6. Study plan 41
3.7. Ethics committee approval 41
4. RESULTS 42
4.1. Induction based modeling – EGF Treatment 42
4.1.1. EGF treatment causes morphological changes. 42
4.1.2. EGF treatment causes neuroendocrine differentiation. 43
4.1.3. EGF treatment affects proliferation, colony formation and spheroid formation. 47
4.1.4. EGF treatment affects the cell invasion capability 50
4.1.5. EGF affects the cell cycle and cause G0/G1 arrest 51
4.1.6. EGF affects the neuroendocrine differentiation related gene expression. 53

4.1.7. EGF treatment induces EMT. 54
4.1.8. EGF activates Akt-Erk pathway in bladder cancer cells. 56
4.1.9. EGF treatment downregulates CAV1. 58
4.1.10. EGF treatment increases nuclear localization of β-catenin. 59
4.1.11. EGF induce the WNT signaling pathway. 61
4.2. Gene Editing/ Gene-Character Change Based Neuroendocrine Modeling 62
4.2.1. Establishment of Mutations by CRISPR/Cas9 HDR 63
4.2.2. In Vitro Cleavage assay shows that Cas9 and sgRNA works properly. 63
4.2.3. Overexpression of Mutant Genes 65
4.2.3.1. PHAGE-KRAS-G12D plasmid was transduced to SV-HUC-1 cell line using lentiviral transduction. 65
5. DISCUSSION 66
6. CONCLUSION AND FUTURE ASPECTS 67
7. REFRENCES 68
8. APPENDİX ..... 77 8.1. Research Ethics Committee Approval 77

INDEX OF FIGURES

Figure 1 Molecular subtype classifications of bladder cancer) 6
Figure 2 Canonical WNT/ B-catenin signaling 10
Figure 3 Hypothesis of origin of neuroendocrine tumors 13
Figure 4 MAPK/Erk-PI3K/Akt pathway 15
Figure 5 IL6 regulation of neuroendocrine differentiatio 16
Figure 6 Map of mutant KRAS, ARID1A and CTNNB1 plasmids. 39
Figure 7 Brightfield images of T24 and 5637 cell lines 43
Figure 8 Immunofluorescence staining images of ENO2 staining 45
Figure 9 qRT PCR result of ENO2 expression 45
Figure 10 Immunofluorescence staining results of ChgA staining 46
Figure 11 Cell proliferation analysis. 47
Figure 12 Colony formation images and analysis. 48
Figure 13 Spheroid formation images and bar plots 49
Figure 14 Scratch assay images and quantitively analysis 51
Figure 15 Cell cycle arrest analysis of T24 and 5637 cell line 52
Figure 16 q-RT PCR analysis of neuroendocrine differentiation related genes 54
Figure 17 Immunofluorescence images and analysis of E-cadherin staining 55
Figure 18 Akt/Erk pathway activation analysis 57
Figure 19 Western blot result of CAV1 58
Figure 20 Immunofluorescence staining showing the nuclear localization β-catenin)60
Figure 21 WNT reporter assay analysis of T24 and 5637 cell lines. 61
Figure 22 Mutation analysis in neuroendocrine-like bladder cancer 62
Figure 23 Mutations in CTNNB1, KRAS and ARID1A genes in neuroendocrine-like

bladder cancers. 63
Figure 24 In vitro cleavage assay gel images..... 64
Figure 25 In vitro cleavage incubation time optimization. 64
Figure 26 Flow cytometry analysis of PHAGE-KRAS-G12D transduced SV-HUC-1 cell line. 65

INDEX OF TABLES

Table 1 Laboratory equipment used in this thesis and their supplier companies 17
Table 2 Laboratory supplies used in this thesis and their supplier companies..... 18
Table 3 Commercial kits used in this thesis and their supplier..... 19
Table 4 Solutions used in cell culture experiments 19
Table 5 General chemicals used in this thesis 20
Table 6 TBS Components (10X / 1L) pH~7,6..... 21
Table 7 TBST Components (1X/1L) 22
Table 8 RIPA Buffer Components (1X/100 ml)..... 22
Table 9 Running Buffer Components (10X / 1L) pH~8,3..... 22
Table 10 Transfer Buffer Components (10X / 1L) pH~8,3..... 22
Table 11 Laemmli Buffer Components..... 23
Table 12 Ponceau Dye Components 23
Table 13 Plasmids used for WNT reporter assay in this thesis and their companies 23
Table 14 Components of Agar Plates (for 1L)..... 24
Table 15 Components of LB Medium (for 1L) 24
Table 16 Antibodies used in this thesis and their supplier companies 24
Table 17 qRT-PCR primers and their sequences used in this thesis 25
Table 18 gRNA used for CRISPR-Cas9 HDR experiment in this thesis..... 25
Table 19 Components of Cas9 Nuclease Reaction Buffer (10X, pH=7.9 at 25°C) 26
Table 20 Components of Cas9 Dilution Buffer 26
Table 21 Enzymes used for Gene Editing experiments in this thesis..... 27
Table 22 Oligos design for generate overexpression plasmids for this thesis..... 27
Table 23 Plasmids used for overexpression cloning 27
Table 24 Components of FACS buffer 28

ABBREVIATIONS

EMT: Epithelial to mesenchymal transition

MIBC: Muscle invasive bladder cancer

NMIBC: Non muscle invasive bladder cancer

BCG: Bacille Calmette-Guérin

NE: Neuroendocrine

EGF: Epidermal growth factor

EGFR: Epidermal growth factor receptor

IL: Interleukin

PI: Propidium Iodide

CRISPR: Clustered Regularly Interspaced Short Palindromic Repeats

HDR: Homology directed repair

SCNEC: Small cell neuroendocrine cancer

LCNEC: Large cell neuroendocrine cancer

SCPC: Small cell prostate cancer

SCLC: Small cell lung cancer

SCBC: Small cell breast cancer

FBS: Fetal Bovine Serum

PBS: Phosphate Buffer Saline

ACKNOWLEDGEMENTS

First of all, I would like to thank my advisor Doç. Dr. Serap ERKEK ÖZHAN for accepting me into her group and giving me the opportunity to work on this project, for her guidance, patience, help and belief in me. It will always be an honor and pleasure for me to work under her guidance and supervision.

I would also like to thank my co-advisor Doç. Dr. Şerif ŞENTÜRK for his valuable advice, guidance, support, patience, and mentorship throughout this thesis process. I would also like to thank all his lab members for their experience and help.

I would like to thank Prof. Dr. Kutsal YÖRÜKOĞLU for his clinical contributions.

I would like to thank my lab members and friends Burcu AKMAN, Gülden ÖZDEN YILMAZ and Gizem ÖZGÜN for their endless patience, help, and great friendships. I would like to extend my special thanks to Burcu AKMAN for all her help, support, mentorship and for being there for me whenever I had difficulties. Working with her and with her help made everything much easier.

I would like to thank TÜBİTAK for providing financial support and bursary to carry out this project (TÜBİTAK 2247A Young Researcher Program Project no 120C129, EMBO Installation Grant number:4148).

I would like to express my endless love and thanks to my family Meral BOYVATLI, Mehmet BOYVATLI and Kaan BOYVATLI for always being there for me, for their love, support, and trust in me.

I would also like to thank beloved Korhan İSTANBUL for all his support, endless love, patient, and trust in this journey.

Lastly, I would like to thank all my friends at IBG for making this journey much more enjoyable.

Modelling Neuroendocrine Differentiation in Bladder Cancer and Analysis Phenotypic and Molecular Effects

ABSTRACT

Bladder cancer is one of the most common and deathly cancers in the world. Nearly 90% of bladder cancers originates from urothelium. Histopathologically bladder cancer is divided into 2 classes as muscle invasive bladder cancer (MIBC) and non-muscle invasive bladder cancer (NMIBC). Recent consensus classification divide MIBC based on transcriptomic data and neuronal or neuroendocrine-like bladder cancer is one of the classes of MIBC. Neuroendocrine-like bladder cancer shows very bad prognosis and low survival rate. There have been very limited studies about the neuroendocrinelike bladder cancer and almost no studies about the modeling of neuroendocrine-like differentiation in bladder. Primary aim of this study is to generate neuroendocrine-like bladder cancer cell line. For this aim 2 different approaches were used.

The first approach was induction-based neuroendocrine differentiation. In this approach, EGF treatment was used in T24 and 5637 bladder cancer cell lines as EGFR overexpression is frequently seen in bladder cancer, and EGF treatment is commonly used to induce neuroendocrine differentiation in other cancer types. Once the neuroendocrine differentiation was observed, differentiation related gene expression, proliferation and cell to cell interaction analyses were performed. Also, the molecular changes associated with EGF related pathways were analyzed. These analyses showed that after EGF treatment, neuroendocrine differentiation related gene expression was induced, cell proliferation rate was decreased and cell to cell interaction was likely disrupted because of EMT. Also results showed that EGF activate the Akt/Erk pathway. Overall, our findings shows that EGF treatment causes the neuroendocrine differentiation, but further investigations should be performed to understand the mechanism better.

The second approach was gene editing/gene-character change based neuroendocrine differentiation. For this aim, *CTNNB1* mutation and other gene mutations frequently observed in neuroendocrine-like tumors were tried to be

introduced. CRISPR/Cas9-HDR method and overexpression methods are currently used in parallel. Mutation analysis and further phenotypic and molecular analysis will be performed after the mutations are generated in SV-HUC-1 cell line.

Mesane Kanserinde Nöroendokrin Farklılaşmanın Modellenmesi ve

Fenotipik ve Moleküler Etkilerinin Araştırılması

ÖZET

Mesane kanseri dünyada en sık görülen ve en ölümcül kanserlerden biridir. Mesane kanserinin yaklaşık %90'ı ürotelyal kaynaklıdır. Histopatolojik olarak mesane kanseri kasa invaziv mesane kanseri (MIBC) ve kasa invaziv olmayan mesane kanseri (NMIBC) olarak 2 sınıfa ayrılır. Yapılan son konsensus çalışmalar kasa invaziv mesane kanserini transkriptomik verilere dayanarak farklı sınıflara ayırır. Nöronal veya nöroendokrin benzeri mesane kanseri bu sınıflardan bir tanesidir. Nöroendokrin benzeri mesane kanseri kötü prognoza sahiptir ve düşük sağkalım oranı göstermektedir. Nöroendokrin benzeri mesane kanseri hakkında çok fazla çalışma yapılmamıştır ve nöroendokrin benzeri farklılaşmanın modellenmesi hakkında mesanede yapılmış neredeyse hiç çalışma yoktur. Bu çalışmanın birincil amacı nöroendokrin benzeri mesane kanseri hücre hattı oluşturmaktır. Bu amaç için 2 farklı yaklaşım kullanılmıştır.

İlk yaklaşım indüksiyon temelli nöroendokrin farklılaşmasıdır. EGFR'ın aşırı ekspresyonu mesane kanserinde sık olarak görüldüğü ve EGF ile muamele diğer kanser türlerinin nöroendokrin modellenmesinde yaygın olarak kullanıldığı için, bu yaklaşımda iki mesane kanseri hücre hattı, T24 ve 5637 EGF ile muamele edilmiştir. Nöroendokrin farklılaşma gözlendikten sonra, farklılaşma ile ilgili gen ifadesinin, proliferasyon ve hücrelerin birbirleriyle etkileşiminin analizi yapılmıştır. Ayrıca, EGF ile ilgili yolakların nasıl etkilendiği analiz edilmiştir. Bu analizler, nöroendokrin farklılaşmayla ilgili genlerin ifadesinin arttığını, hücre bölünme oranının azaldığını ve EMT nedeniyle hücre-hücre etkileşiminin muhtemelen bozulduğunu göstermiştir.

Ayrıca sonuçlar EGF'in EMT'yi ve Akt/Erk sinyal yolağını aktive ettiğini göstermiştir. Bulgularımız EGF kullanımının nöroendokrin farklılaşmaya neden olduğunu göstermektedir, ancak mekanizmayı daha iyi anlamak için daha fazla araştırma yapılmalıdır.

İkinci yaklaşım gen düzenleme/gen-karakter değişimi temelli nöroendokrin farklılaşmasıdır. Bu amaçla *CTNNB1* mutasyonu ve nöroendokrin benzeri tümörlerde sıklıkla gözlenen diğer gen mutasyonları oluşturulmaya çalışılmıştır. Bu yaklaşımda CRISPR/Cas9-HDR yöntemi ve overekspresyon yöntemleri eş zamanlı olarak gerçekleştirilmeye çalışılmaktadır. SV-HUC-1 hücre hattında mutasyonlar oluşturulduktan sonra mutasyon analizi ve ileri fenotipik ve moleküler analizler yapılacaktır.

1. INTRODUCTION AND AIM

Bladder cancer is one of the most common malignant diseases worldwide. It is also one of the most common causes of cancer-related deaths.(Sanli et al., 2017) Generally, bladder carcinoma is divided into 2 classes, which are urothelial carcinoma and non-urothelial carcinoma. Most of the bladder cancers are urothelial carcinoma. Urothelial carcinoma histopathologically divided into 2 classes: Muscle invasive bladder cancer (MIBC) and non-muscle invasive bladder cancer (NMIBC) (Garg & Maurya, 2019). NMIBC and MIBC are very heterogenous so there has been many studies for transcriptomic classification of MIBC and NMIBC (Fong et al., 2020; Jalanko et al., 2020). Consensus MIBC classification divide MIBC based on transcriptomic data and neuroendocrine-like bladder cancer is one of the classes of MIBC (Kamoun et al., 2020). Neuroendocrine-like type of bladder cancer is rare type of MIBC. It has high a metastasis and low survival rate and mostly have poor outcomes (Grivas et al., 2020). Immunohistochemical analysis is done for Neuroendocrine-like bladder cancer, may not always express classical however they can express intermediate level of neuronal markers. Additionally Neuroendocrine-like tumors overexpress neuronal marker genes but they lowly express basal or luminal marker genes (Al-Ahmadie & Netto, 2019; Da

Costa et al., 2019) Therefore, rather than marker-based classification, transcriptomebased should be used (Da Costa et al., 2019).

There is different hypothesis for the origin of neuroendocrine tumors. One hypothesis is that normal neuroendocrine cells in tissue is origin of NE tumors. The other way is lineage plasticity hypothesis (Y. Wang et al., 2021). Aim of this study is to generate neuroendocrine bladder differentiated cell lines. One approach is to trigger trans differentiation with EGF treatment and analyze phenotypic and molecular effects of the differentiation. Firstly, T24 and 5637 cells, which are bladder cell line without neuroendocrine characteristics, were treated with EGF and after differentiation were generated how the morphology and molecular mechanism would have been affected was analyzed. The other approach is generating neuroendocrine differentiated cell lines by means of certain mutations. KRAS G12D, CTNNB1-S45F and ARID1A W2050* mutations will be generated by CRISPR/Cas9-HDR method or overexpressed mutated genes in SV-HUC-1 cell line.

2. GENERAL INFORMATION

2.1. Bladder Cancer General Characteristics

Bladder cancer is one of the most common malignant diseases and with more than 550.000 new cases and more than 210.000 deaths in 2020. Men are mostly more affected than women as mortality rates and incidence of 3.3 and 9.5 per 100,000 men, respectively and these rates are nearly four times higher than the ones observed women. The biggest risk factor for bladder cancer is age. The average age at diagnosis is between 70 and 84 (Lenis et al., 2020; Sanli et al., 2017; Sung et al., 2021). Exposure to carcinogen like tobacco products and benzene chemicals, long term exposure of arsenic, genetic predisposition, and hormonal imbalance increases the risk of developing bladder cancer (Garg & Maurya, 2019; Sanli et al., 2017)

Most widely bladder carcinoma is divided into 2 classes which are urothelial carcinoma and non-urothelial carcinoma. More than 90% of bladder cancers are urothelial carcinoma(Garg & Maurya, 2019) .

Urothelial carcinoma divided into 2 classes histopathologically: Muscle invasive bladder cancer (MIBC) (stages T2, T3 and T4) and non-muscle invasive bladder cancer (NMIBC) (stages Ta, T1, and Tis)(Fong et al., 2020). Urothelial NMIBC the is most common type of bladder cancer. Nearly 75% of bladder cancer tumors are NMIBC tumors (Ahmad et al., 2011). NMIBC has better prognosis, and it is not generally a threat to survival, but recurrence rate is high (McConkey & Choi, 2018). On the other hand, MIBC is more aggressive and shows worse prognosis than NMIBC. Diagnosis of MIBC is generally de nova but 10-20% of the MIBC may arise from NMIBC.

Approximately 25% of bladder tumors contain variant histology. This can present therapeutic challenges and unique diagnostic that are critical to the management of bladder cancer (Black & Black, 2020). Generally, MIBC is treated with cisplatin-based chemotherapy followed by radial cystectomy, but nowadays neoadjuvant chemotherapy (NAC) is also given in additional to cisplatin-based chemotherapy. However only 20% of the MIBC patients have chance to take NAC in clinical trials. (Iacovino et al., 2022). On the other hand, high-risk or intermediate-risk NMIBC patients are given Bacille Calmette-Guérin (BCG) treatment (Lenis et al., 2020). If NMIBC patient is suitable for cystectomy, it is the best option for treatment. If the patient is not eligible for cystectomy, aggressive repeated transurethral resection of the bladder tumor (TURBT) is recommended (Black & Black, 2020).

Overall mutation rate in MIBC is higher than NMIBC (Kamoun et al., 2020; Ringuette-Goulet et al., 2018). Also, MIBC can rapidly progress and become metastatic to the lymph nodes, brain, liver, bones and lungs, often resulting in death (McConkey & Choi, 2018). NMIBCs are heterogeneous in their propensity to progress to MIBC and their response to available therapies, making NMIBC a heterogeneous disease. (Fong et al., 2020). Because of the high mutation rate and genomic instability, MIBC is also a very heterogenous disease. Because of the heterogeneity, MIBC and NMIBC are divided into different molecular subgroup with different classification methods (Jalanko et al., 2020).

2.1.1. Molecular Characterization of Bladder Cancer

In recent years, there has been an increase in the number of studies on molecular characterization of cancer to improve diagnostic criteria (Fong et al., 2020). Studies have been carried out on the molecular characterization of bladder cancer using different methods and different approaches such as UROMOL, Baylor, University of North Carolina (UNC), MD Anderson Cancer Center (MDA), the Cancer Genome Atlas (TCGA), Cartes d'Identité desTumeurs (CIT)-Curie and Lund.Genomic

characterization has shown that Activating FGFR3 mutations, diploid or near diploid karyotypes are characteristic features of most NMIBC. In contrast, frequent *TP53*, *RB1* and *PTEN* mutations, aneuploidy and multiple chromosomal alterations are characteristic features of majority of MIBC (Chandrasekar et al., 2018; Tan et al., 2019).mRNA expression based molecular subtyping is the most common way of classification, used in many publications. (Kamoun et al., 2020; Lindskrog et al., 2021; Robertson et al., 2017).

Two recent studies provided consensus classification for both NMIBC and MIBC. In this respect, NMIBC divided into 4 classes which are class 1, class 2a, class 2b and class 3 by analyzing UROMOL 2021 data (Lindskrog et al., 2021). MIBC is classified in 6 biologically relevant consensus: "Luminal papillary (LumP)", "Luminal nonspecified (LumNS)", "Luminal unstable (LumU)", "Stroma-rich", "Basal- squamous (Ba/sq) "and "Neuroendocrine-like (Ne-Like)" (Kamoun et al., 2020). With 35% sample size, basal-squamous is the largest subgroup of MIBC. On the contrary, with 3% sample size, neuroendocrine-like MIBC is the smallest subgroup (Kamoun et al., 2020; Robertson et al., 2017).

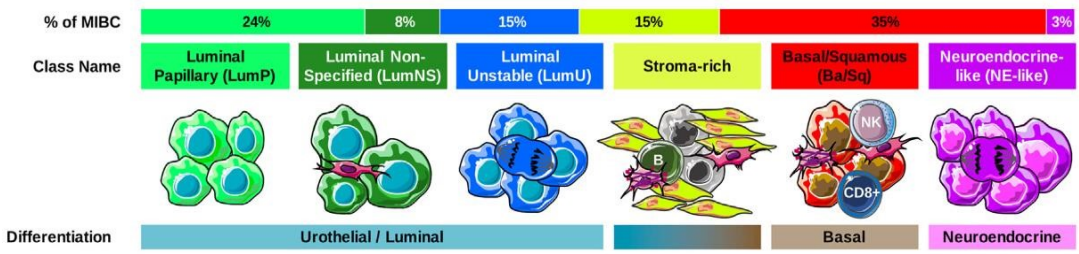


Figure 1 Molecular subtype classifications of bladder cancer (edited by (Kamoun et al., 2020))

Each MIBC subtype has significant characteristics. Urothelial differentiation signature genes like *GATA3, PPARG*, FOXA*1* and uroplakins (*UPK2* and *UPK1A*) are overexpressed in luminal classes. On the contrary, basal, and neuroendocrine differentiation related gene signatures and *TP53* and *RB1* genes are overexpressed in basal-squamous and neuroendocrine-like tumors (Fong et al., 2020; Jalanko et al., 2020; Kamoun et al., 2020).

Beyond this, three luminal classes have distinct and specific characteristics. High expression of non-invasive Ta pathway signatures is characteristic of luminal papillary tumors. Also, luminal papillary tumors are highly associated with FGFR3 transcriptional activity. Luminal non-specified tumors show high stromal infiltration signatures. Compared to other two luminal tumors, luminal unstable displays high cell cycle activity compared to other luminal classes. Stroma-rich tumors have intermediate level of urothelial differentiation, but stromal infiltration is their signature characteristic. Basalsquamous tumors also show stromal infiltration as a characteristic feature. On the other hand, neuroendocrine tumors show no transcriptomic markers of immune infiltration (Kamoun et al., 2020).

2.1.2. Neuroendocrine Subtype of Bladder Cancer

As mentioned above, neuroendocrine, and neuroendocrine-like type of bladder cancer is rare type of MIBC but mostly have poor outcomes just neuroendocrine bladder cancer. It has a high metastasis and low survival rate (Grivas et al., 2020) Neuroendocrine bladder cancer may present at diagnosis as pure neuroendocrine lesions or, more frequently, coexist with classic urothelial cell carcinomas. Studies have shown that neuroendocrine tumors can arise de novo or develop through lineage transmission (Shen et al., 2018). According to the classification of bladder cancer tumors by WHO in 2016, bladder neuroendocrine carcinoma includes large cell

neuroendocrine carcinoma (LCNEC), small cell neuroendocrine carcinoma (SCNEC), paraganglioma and well-differentiated neuroendocrine tumor (Moschini et al., 2017). Among these four subtypes, small cell neuroendocrine carcinoma is the most common subtype, but it just accounts for 1% of all bladder cancer and LCNEC is the rarest (Xia et al., 2020).

Neuroendocrine tumors are usually small, round, and malignant cells. On the other hand, Neuroendocrine-like tumors generally irregular cluster of large tumor cells and have nuclear pleomorphism (Da Costa et al., 2019) . In neuroendocrine class of bladder cancer, necrosis in the form of coagulative or apoptotic bodies is commonly observed. This type is most aggressive one in bladder cancer. Mostly show worse prognosis, metastasis, and low 5-year of survival rate (Moschini et al., 2017).

Because morphology of neuroendocrine tumors is not completely clear, immunohistochemical markers are used as a diagnostic confirmation (Black & Black, 2020). On the other hand, NE-like tumors are morphologically like other urothelial carcinoma but show similar transcriptomic profiles and genotypes to neuroendocrine tumors (Da Costa et al., 2019; Grivas et al., 2020). Neuroendocrine-like tumors generally do not express classic markers of NE differentiation like chromogranin A or synaptophysin, they can express intermediate level of neuronal markers like SOX2 or PEG10 (Da Costa et al., 2019). So, morphologically, or marker-based classification is not completely correct or enough. Transcriptomic analysis should be used.

Neuroendocrine bladder cancer has high mutation rate like 12.91 base per million base pair (Shen et al., 2018). C to T conversions is observed in the mutation spectra of most of the sequenced neuroendocrine samples and mostly mutated genes are *TP53, PIK3CA, RB1, EP300, ARID1A, and ERCC2* which are already defined other classes of bladder cancer (Shen et al., 2018). Loss of *RB1* and *TP53* support NE transition (Da Costa et al., 2019). Unlike mutation analysis, gene expression profiles of neuroendocrine-like tumors show differences from other classes of bladder cancer. In neuroendocrine- like tumors, neuronal marker genes for example NESTIN, TUBB2B, PEG10, PLEKHG4 are overexpressed however show low or no express of basal or

luminal marker genes such as *FOXA1, GATA3, KRT5,* and *KRT14* (AlAhmadie & Netto, 2019; Da Costa et al., 2019).

In low stage of bladder cancers, no N-cadherin expression and high E-cadherin expression is seen but in high stage of bladder cancers, the opposite situation is observed (Plissonnier et al., 2011). Because the increase in N-cadherin expression and loss of E-cadherin expression is frequently seen in migration and invasion. This regulation is regarded as one of hallmarks of epithelial to mesenchymal transition in cancer. When E-cadherin expression is downregulated, epithelial cell junctions are disrupted, and cancer cells can easily metastasis. On the contrary of E cadherin down regulation, upregulation of N-cadherin has a role in increased cell motility. (Mrozik et al., 2018). N-cadherin expression is identified to be high while E cadherin expression is low in neuroendocrine-like bladder cancers (Eray et al., 2020; Plissonnier et al., 2011). Additionally, β-catenin/WNT pathway has been determined to be activated in neuroendocrine-like bladder cancer (Eray et al., 2020; Tan et al., 2019).

2.2. Role of β-catenin Dependent Wnt Pathway in Cancer

WNT pathway is an important pathway for regulation of many processes like differentiation embryonic development, cell migration, cancer progress, EMT process, tissue homeostasis, cell proliferation (Garg & Maurya, 2019; Grossmann et al., 2012). Wnt signaling pathway components have been implicated as important diagnostic and prognostic markers and novel therapeutic targets.(Garg & Maurya, 2019).

WNT signaling pathway is divided into 2 signaling branches. The first pathway is called canonical pathway also called β-catenin dependent. Second one is noncanonical pathway known as β-catenin independent pathway (Liu et al., 2014). Non canonical WNT pathway regulate cell polarity (Bian et al., 2020). Canonical WNT signaling has a role of survival, proliferation, and differentiation related gene regulation (Grossmann et al., 2012). If there is a disfunction, dysregulation or mutation of WNT/ β-catenin signaling, tumorigenesis, malignancy and cancer immunotherapy failure can be occurred (Garg & Maurya, 2019; Kim et al., 2013; Wen et al., 2020)

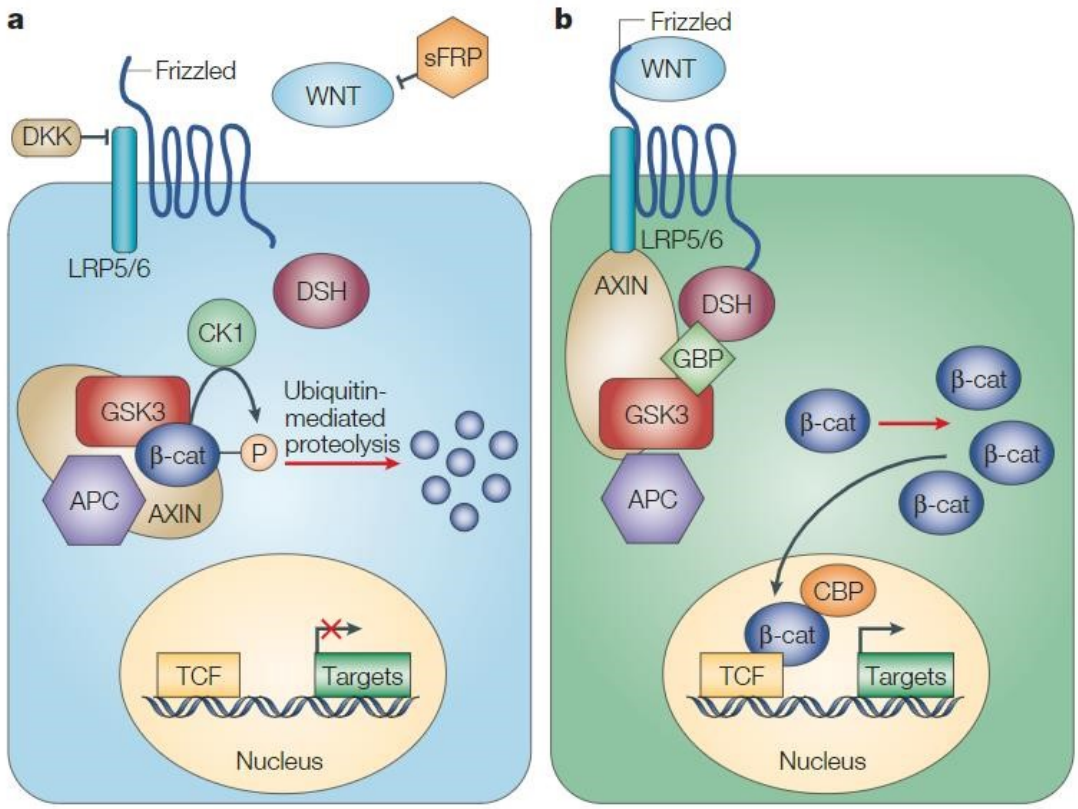


Figure 2 Canonical WNT/ B-catenin signaling a) WNT is absent b) WNT is present (Edited by (Moon et al., 2004))

In the absence of WNT, β-catenin is sequestered in a degradation complex consisting of APC, Axin, CK1α and GSK3β. Consequently, β-catenin is degraded by phosphorylation and ubiquitination by destruction complex. Cytoplasmic β-catenin levels are not increased and WNT target genes are repressed (Grossmann et al., 2012; Heuberger & Birchmeier, 2010). In the presence of WNT, the activity of degradation complex is inhibited upon WNT interaction with Frizzled/LRP. β-catenin accumulates in the cytoplasm and influx to the nucleus, recruit coactivators, CBP and BCL9, and interact with TCF/LEF protein. As a result, WNT target genes *c-myc*, *FGF, EGF, Cyclin D1, CD44* are activated. (Garg & Maurya, 2019; Grossmann et al., 2012; Wen et al., 2020).

β-catenin-TCF/LEF1 activity can also be regulated many ways independent of GSK3β (Lu et al., 2003).For instance EGF upregulation downregulate cell to cell

adhesion and cause EMT and caveolin mediated endocytosis of E-cadherin. Ecadherin downregulation leads to disrupt E-cadherin/β-catenin complex and leads to release β-catenin into the cytoplasm and finally translocate to the nucleus (Heuberger & Birchmeier, 2010; Lu et al., 2003). Whether independent or dependent of GSK3β, overactivation of WNT signaling induce Wnt dependent tumor formation (Bugter et al., 2021).

2.3. Role of EGF Signaling in Cancers

Epidermal growth factor receptor (EGFR) is one of the most important and complex signaling molecules in biological processes. It has many crucial roles in development, homeostasis, proliferation, and apoptosis. Aberrant activation of EGFR may lead to tumorigenesis and cancer development (Sijia Wang, 2019).

EGFR is a main factor in malignancies and most altered oncogene in solid cancer types (Sasaki et al., 2013; Thomas & Weihua, 2019). There are 2 types of pathological alterations in EGFR in cancer which are kinase-activating mutation and EGFR overexpression. Overexpression of EGFR is much more commonly seen than kinaseactivating mutation (Thomas & Weihua, 2019).

Aberrant EGFR signaling enhances the tumor growth, migration, metastasis, and invasive characteristics in many cancers type through different pathways like PI3K and ERK pathway (Uribe et al., 2021). Downstream of EGFR, Ras-ERK enhance invasiveness and migration, causing EMT. EGFR overexpression has been described in various tumors. For example, breast cancer, prostate cancer, non-small cell lung cancer and bladder cancer tumors. Expression of EGFR ligands and EGFR is associated with metastasis, cancer proliferation and survival (Huang et al., 2019). In breast cancer, EGFR overexpression is seen in aggressive types. Poor clinical outcomes and large tumor size are observed (Masuda et al., 2012). In bladder cancer, tyrosine-kinase receptors, which include many growth factor receptors such as epidermal growth factor receptor (EGFR), are overexpressed in urothelial tumors. The level of expression of EGFR and its ligand is correlated with tumor grade, tumor stage and cancer progression (Bellmunt et al., 2003; Mooso et al., 2015).

Inhibition of EGFR signaling pathways and EGFR kinase activity with different drug combinations like Akt/ERK or PI3K can be a good therapeutic strategy for cancer patients (Sasaki et al., 2013).

2.4. Modelling of Neuroendocrine Cancers

2.4.1. Origin of Neuroendocrine Tumors

Origin of neuroendocrine tumors can be different. Their origin is still unknown, but studies point to two different hypotheses. One hypothesis is based on neuroendocrine cell hypothesis which is that normal neuroendocrine cells in tissue is origin of NE tumors. Neuroendocrine cells show malignant transformation and become NE tumors. It is called de novo neuroendocrine cancer and it is seen very rare (Y. Wang et al., 2021). The other hypothesis is the lineage plasticity hypothesis. In lineage plasticity, cells can differentiate, they can lose the adenocarcinoma cell characteristics and obtain neuroendocrine phenotype. It is observed more often than neuroendocrine cell hypothesis (Y. Wang et al., 2021; Yang et al., 2020).

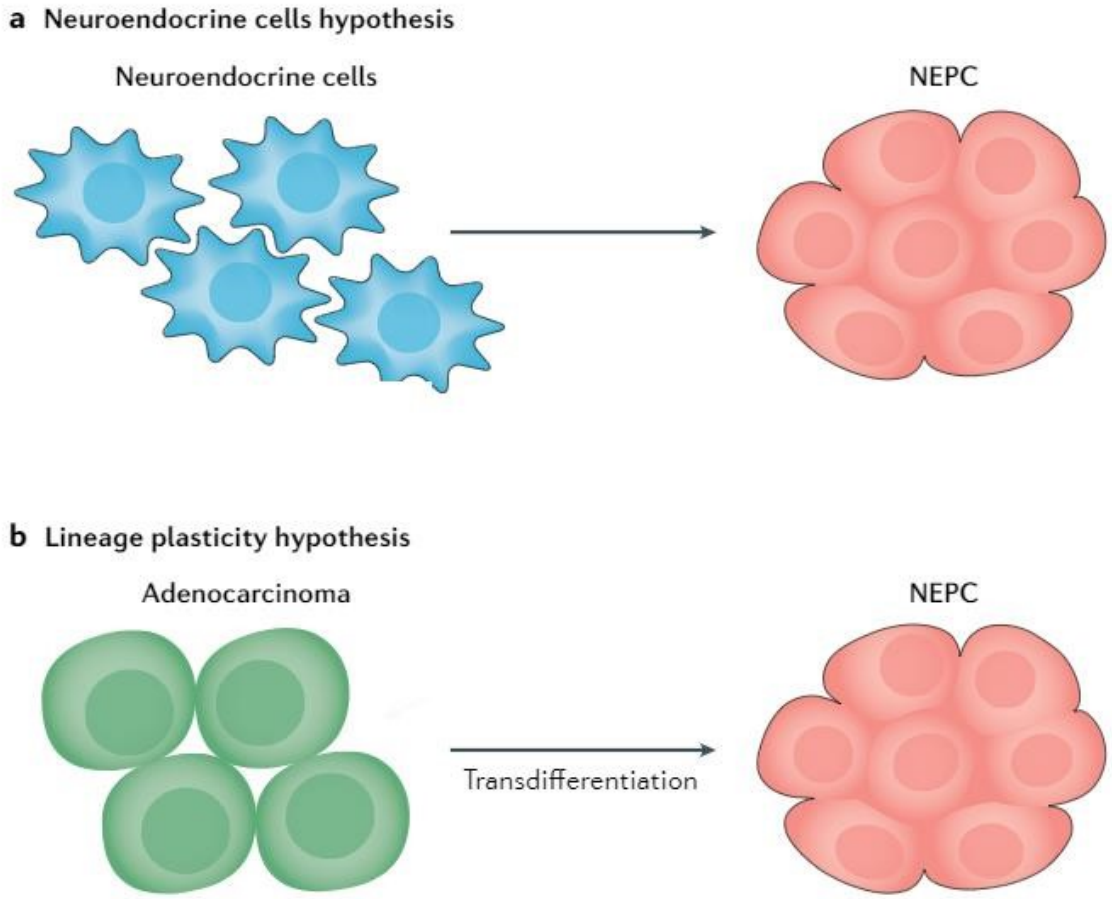


Figure 3 Hypothesis of origin of neuroendocrine tumors (Adapted from (Y. Wang et al., 2021))

In the lineage plasticity, urothelial differentiation genes are downregulated, but the genes related to neuronal differentiation are overexpressed. For example, transcriptionally small cell prostate cancer (SCPC) and small cell lung cancer (SCLC) share similarities rather than their origin of normal epithelial cells such as they share common genetic alterations like loss of *RB1* gene and mutation of *TP53*. Genome editing, therapies or treatment with cAMP, growth factors or interleukins induce lineage plasticity trans differentiation. Analysis show that neuroendocrine-like bladder cancer and other bladder cancer molecular subtypes share some similar copy number variations, genetic alterations, and origin cells. This argues that neuroendocrine tumors

originate from adenocarcinoma (Dong et al., 2020; L. Wang et al., 2020; Y. Wang et al., 2021).

2.4.2. Gene Editing/ Gene-Character Change Based Approaches

Modeling of neuroendocrine tumors can be achieved different ways. One way is based on gene editing or changing gene character. In this approach epithelial cells to small cell carcinoma are induced with some mutations. In some studies, specific set of genetic factors induce neuroendocrine tumors initiation in epithelial cells (L. Wang et al., 2020). These genetic factors are dominant negative form of TP53, myristoylated AKT1, RB1 shRNA, c-myc and BCL2 which are all together referred as PARCB. All the PARCB tumors which derived from basal cells share some similarities like high nuclear to cytoplasmic ratio or expression of NED markers (Park et al., 2018; L. Wang et al., 2020). From lung or prostate epithelial cells or normal urothelial cells, PARCB factors can generate SCLC or SCPC or SCBC (Park et al., 2018; L. Wang et al., 2020). This method can be used as one way to generate neuroendocrine differentiated bladder cancer cell lines. Other than this study, there are not really known example of geneediting or gene character change-based neuroendocrine differentiation in literature.

2.4.3. Induction Based Methods

Neuroendocrine differentiation can be induced by many methods. Exposition to growth factors such as EGF, Interleukins like IL6, hypoxia, radiation or metals can result in neuronal differentiation (Y. Chang et al., 2013; Delk & Farach-Carson, 2012; Deng et al., 2008; Lin et al., 2016; Soh et al., 2012). Application of these different factors activates distinct pathways, and effect different metabolic processes. For instance, it has been known that EGF regulate differentiation role in prostate cancer (Cortés et al., 2012). EGF receptor induction cause many signaling pathways in cytoplasm like MAPK and PI3K/Akt pathway. Aberrant activation of Akt/Erk pathway cause neuroendocrine differentiation(Cortés et al., 2012; Xie et al., 2022).

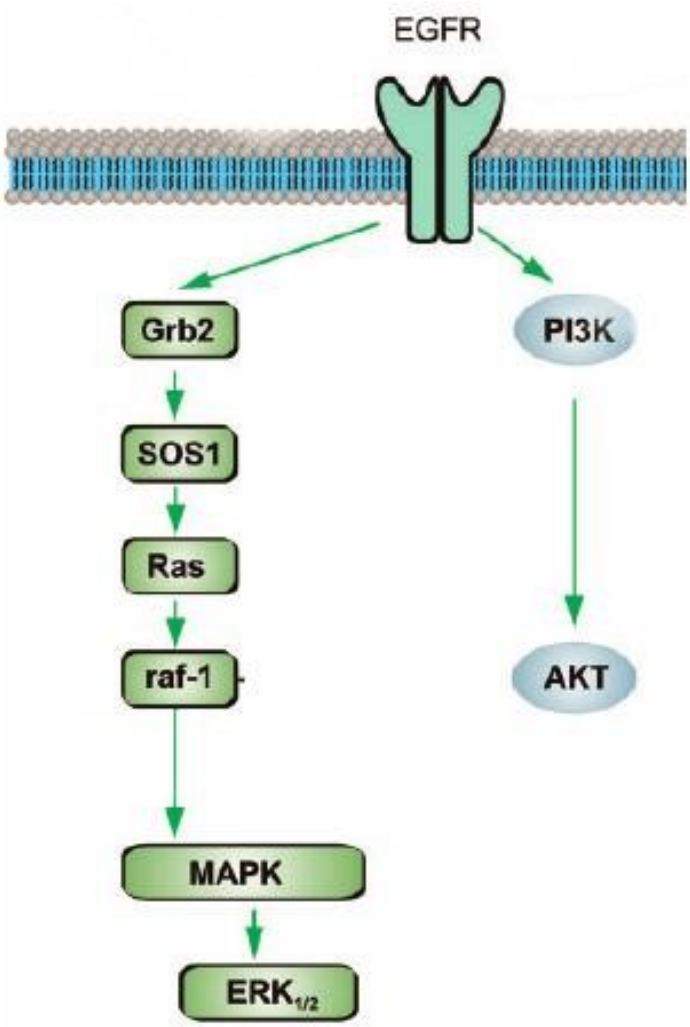


Figure 4 MAPK/Erk-PI3K/Akt pathway (Adapted from (Zhou et al., 2015))

IL6 treatment can also induce neuroendocrine differentiation through different signaling pathway like activation of STAT3 pathway (K.-T. Chang et al., 2005). In prostate cancer it has been known that IL6 has paracrine factor role, and it can inhibit the cell growth and induce neuroendocrine differentiation. STAT3 signaling pathway is a mediator of this differentiation process. Studies reveal in the absence of STAT3

activity IL6 mediated neuroendocrine differentiation is lost. (Spiotto & Chung, 2000; Zhu et al., 2014).

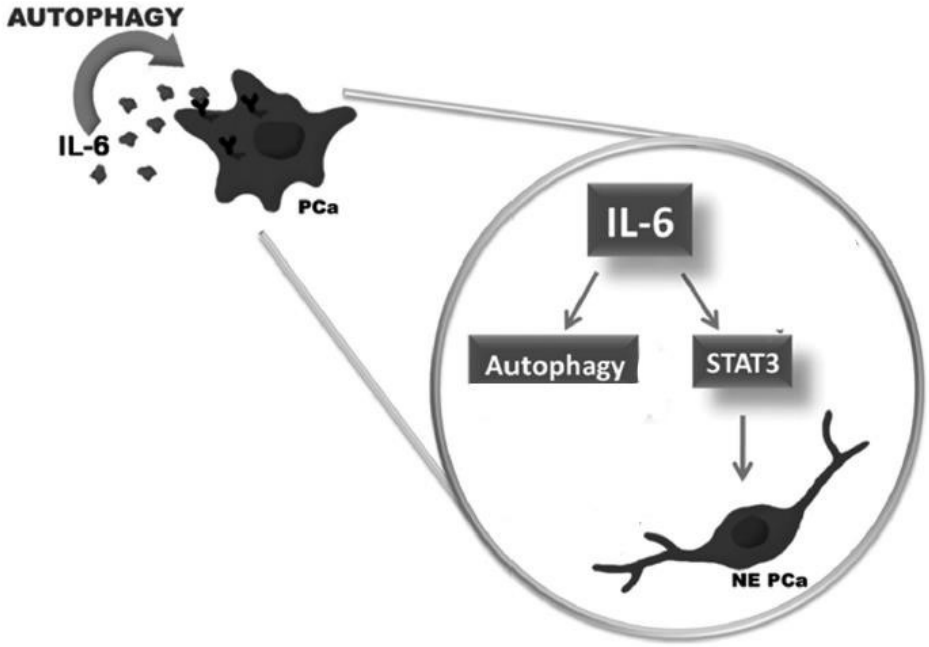


Figure 5 IL6 regulation of neuroendocrine differentiation (Adapted from (Delk & Farach-Carson, 2012)

3. MATERIALS AND METHODS

3.1. Type of The Research

Experimental research.

3.2. The Time and The Place of The Research

This thesis project was done at Izmir International Biomedicine and Genome Center between 2021-2023.

3.3. Research Materials

This thesis was done using 5637, T24, HEK293T and SVHUC-1 cell lines. T24 cell line were kindly provided by Prof. Neşe ATABEY. 5637 purchased from German

Collection of Microorganisms and Cell Cultures GmbH (DSMZ). HEK293T and SVHUC-1 cell lines were kindly provided form Doç. Dr. Şerif ŞENTÜRK.

3.3.1. Laboratory Equipment and Supplies

Laboratory equipment and supplies used in this thesis and their supplier companies are listed in Table 1 and 2.

Table 1 Laboratory equipment used in this thesis and their supplier companies.

Equipment	**Company**
Micropipettes	2 µl, 10 µl, 20 µl, 200 µl, 1000 µl Gilson
Microcentrifuge	Thermo Scientific Micro CL 17R 230 V.
PowerPac™ Basic Power Supply	Bio Rad
Mini Electrophoresis System	Thermo Scientific OWL B1A
Centrifuges	Eppendorf 5810 R
Human Cell Culture Incubator	memmert
Nanodrop	Thermo Scientific Nanodrop 2000
Class II Biological Safety Cabinets	Thermo Scientific Safe 2020
Benchtop Orbital Shaker	Thermo Scientific MaxQ 4000
Water Tank	Nuve NB9
Light Microscope	ZEISS Vert.A1
Inverted Microscope	Olympus CKX41
Fluorescence Microscope	Olympus BX61
Cell Sorting	BD FACSAria III
Flow Cytometer and Cell Analysis	LSR Fortessa
Stereo Microscope	Leica
Microplate Spectrophotometer	Thermo Scientific Multiskan GO
Western Blot System	BIO-RAD
Electronic pipettor	ISOLAB
Thermal Cycler	Simpleamp A24811

Mini Vortex Mixer	Thermo Scientific ELED-88880018/ LPMixer
Micro Centrifuge	Thermo Scientific TS-75004061 mySPIN
Real-Time PCR System	Applied Biosystems 7500 Fast
Western Blot Membrane Imaging System	LI-COR ODYSSEY CLx
Gel Documentation System	BIO-RAD Gel Doc XR+

Table 2 Laboratory supplies used in this thesis and their supplier companies.

Supplies	**Company**
Cell culture dishes	Corning
MicroAmp™ Fast Optical 96-Well Reaction Plate	Thermo Fisher Scientific 4346906
Multiwell plates	Corning
Vacuum filtration system	Milipore
Falcons (15 ml, 50 ml)	SPL
PCR tubes	Neptune
Serological Pipettes	SPL
Eppendorf tubes (0.5 ml, 1.5 ml, 2 ml)	Thermo
Disposable pipette tips	Neptune
Nitrocellulose membrane	BIO-RAD
Color Prestained Protein Standard	NEB P7719S
Glass Pasteur Pipette	ISOLAB
DNA LoBind Tube (1.5 ml)	Eppendorf
Cover Glasses	NEST 801010

3.3.2. Commercial Kits

Commercial kits used in this thesis and their supplier companies are listed in Table 3

Table 3 Commercial kits used in this thesis and their supplier.

Kit	**Company**
Pierce™ BCA Protein Assay Kit	ThermoFisher Scientific 23227
FastStart Essential DNA Green Master	Roche 06402712001
Cell Proliferation Kit I (MTT)	Roche 12352200
Lipofectamine 3000 Reagent	ThermoFisher Scientific L3000001
Maxima First Strand cDNA Synthesis Kit for RT-qPCR	ThermoFisher Scientific K1642
Monarch Total RNA Miniprep Kit	New England Biolab T2010
HiScribe™ T7 Quick High Yield RNA Synthesis Kit	New England Biolab E2050
RNA Clean & Concentrator-25	Zymo Research R-1017
PCR clean-up Gel extraction	Macherey-Nagel 740609.50
Q5® Hot Start High-Fidelity 2X Master Mix	New England Biolab M0494S
Plasmid DNA Purification (Mini)	Macherey-Nagel 740588.50
Dual-Glo® Luciferase Assay System	Promega E2920

3.3.3. Cell Culture

Cell culture media and solutions used in this thesis are listed in Table 4.

Table 4 Solutions used in cell culture experiments.

Solutions	**Company**
Roswell Park Memorial Institute (RPMI) Medium	Gibco 11875101
Dulbecco's Modified Eagle Medium (DMEM)	Gibco 11965092

Fetal Bovine Serum (FBS)	Thermo Fisher Scientific 10500064
Penicillin/Streptomycin	Thermo Fisher Scientific 15140122
Phosphate-Buffered Saline (PBS)	Thermo Fisher Scientific 70011036
TrypLE	Thermo Fisher Scientific 12604013
Opti-MEM	Thermo Fisher Scientific 31985062
Human Recombinant EGF Protein	Thermo Fisher Scientific PHG0311

3.3.4. General Chemical

General chemicals used in this thesis are listed in Table 5.

Table 5 General chemicals used in this thesis

Chemical	**Company**
EDTA	Sigma-Aldrich SRE0033-1L
Ethanol	Merck 100983.2511
Methanol	Sigma-Aldrich 32213-2.5L
NaCl	Sigma-Aldrich S5886-500G
Glycerol	Sigma-Aldrich G9012-100ML
Phosphate Buffer Saline (10X)	Thermo Fisher 70011036
TritonX-100	Sigma-Aldrich T8787-100ML
Na deoxycholate	Sigma-Aldrich D6750-10G
SDS	Invitrogen 24730020
Tris	Sigma-Aldrich 648314-100ML
EGTA	Sigma-Aldrich 324626-25GM
Protease inhibitor coctail	Roche 11836153001
Glycine	Sigma-Aldrich G7403-100G
HCl	Sigma-Aldrich 320331-500ML
Tween-20	Sigma-Aldrich P1379-100ML
Ponceau	Sigma-Aldrich P3504-10G
Acetic Acid	Sigma-Aldrich 27225-2.5L-R
Formaldehyde	Sigma-Aldrich 252549-1L

Tris Acetate-EDTA (TAE) Buffer (10X)	Sigma-Aldrich T9650-1L
Agarose	Sigma-Aldrich A9539-100G
Isopropanol	Sigma-Aldrich 563935-1L
Bromophenol blue	Sigma-Aldrich B0126-25G
TEMED	Sigma-Aldrich 1107320100
10% APS	Biofroxx 1610GR100
Protogel	National Diagnostics EC-891
Skim milk powder	Sigma-Aldrich 70166-500G
Normal Goat Serum	Cell Signaling 5425S
ProLong™ Diamond Antifade Mountant	Invitrogen P36965
DAPI	Sigma-Aldrich D9542
Crystal violet	Sigma-Aldrich V5265
Alt-R® Cas9 Electroporation Enhancer	IDT 1075915
Alt-R™ HDR Enhancer V2	IDT 10007910
Polybrene	Sigma-Aldrich TR-1003-G
Propidium iodide	Invitrogen P3566

3.3.5. Western Blots Buffers

Buffers' components which used in Western Blot experiment are listed in Table 6, Table 7, Table 8, Table 9, Table 10, Table 11, and Table 12.

Table 6 TBS Components (10X / 1L) pH~7,6

Component	**Amount**
Trizma HCl	24.23 g
NaCl	80.06 g

Table 7 TBST Components (1X/1L)

Component	**Amount**
TBS (10X)	100 ml
dH2O	900 ml
Tween-20	1 ml

Table 8 RIPA Buffer Components (1X/100 ml)

Component	**Amount**
Triton X-100 (10%)	10 ml
Na deoxycholate (10%)	4.5 ml
SDS (20%)	500 µl
Tris-Cl pH 7,4 (1M)	5 ml
NaCl (5M)	3 ml
EDTA pH 8 (0,5M)	200 µl
EGTA (0,1M)	100 µl
Protease Inhibitor Cocktail (for 1 ml)	40 µl

Table 9 Running Buffer Components (10X / 1L) pH~8,3

Component	**Amount**
250 mM Tris base	30.2 g
1,9 M Glycine	142 g
1% SDS	

Table 10 Transfer Buffer Components (10X / 1L) pH~8,3

Component	**Amount**
250 mM Tris base	3.02 g
1,9 M Glycine	14.2 g
20% methanol (add before use)	200 ml

Table 11 Laemmli Buffer Components

Component	**Amount**
0.5 M Tris-HCl (pH=6.8)	20 ml
Glycerol	20 g
SDS	4 g
Bromophenol Blue	0.05 g
1M DTT	2 ml
dH2O	13 ml

Table 12 Ponceau Dye Components

Component	**Amount**
Acetic Acid	0.5 ml
Ponceau	0.25 ml
dH2O	**50 l**

3.3.6. Plasmids used for WNT Reporter Assay

587 pGL3.BAR and pGL4.73[hRluc/SV40] plasmids were kindly provided by Prof. Dr. Güneş ÖZHAN and pGL3-Basic plasmid were kindly provided by Doç. Dr. Şerif ŞENTÜRK.

Table 13 Plasmids used for WNT reporter assay in this thesis and their companies.

Plasmid	**Company**	**Catalog no**
pGL4.73[hRluc/SV40]	Promega	E6911
pGL3-Basic	Whatman plasmid	E1751
587 pGL3.BAR		

3.3.7. Bacteria

Bacteria were spread on Bacteriological Agar plates which contain 1X Ampicillin antibiotic and grown in LB medium that contains 1X Ampicillin antibiotic. Components of bacteriological agar plates are shown in Table 14 and Table 15, respectively**.**

Table 14 Components of Agar Plates (for 1L).

Component	**Amount**	**Company**
Bacteriological Agar	35 g	Caisson Labs LBP04-500GM
Ampicillin (1000X)	1 ml	BioFroxx
ddH2O	1 L	-

Table 15 Components of LB Medium (for 1L).

Component	**Amount**	**Company**
Tryptone	10 g	Biolife
Yeast Extract	5 g	Sigma-Aldrich R8508
NaCl	10 g	Sigma-Aldrich S5886
ddH2O	950 ml	-

3.3.8. Antibodies

Antibodies used in this thesis listed in Table 16.

Table 16 Antibodies used in this thesis and their supplier companies.

Antibody	**Company**
B-catenin	Cell Signaling Technology #9562
B-actin	Cell Signaling Technology #4970
E-cadherin	Cell Signaling Technology #3195

ChgA	Cell Signaling Technology #85798S
ENO2	Cell Signaling Technology #65162S
Akt	Cell Signaling Technology #CS9272
Erk1/2	Cell Signaling Technology #CS1696
Cav1	Cell Signaling Technology
Anti-rabbit IgG (Alexa Fluor® 594 Conjugate)	Cell Signaling Technology #8889S
Seconder Antibody	

3.3.9. qRT-PCR primers

Table 17 qRT-PCR primers and their sequences used in this thesis.

Primer Name	**Forward Primer**	**Reverse Primer**
Cav1	ACGTAGACTCGGAGGGACA	GCGTCGTACACTTGCTTCTC
GATA3	TCGCAGAATTGCAGAGTCGT	GAGTTTCCGTAGTAGGGCGG
KLF7	ACCACTGCGACAGGTGTTTTT	GCCTCATGGCGTTTCCTTTAG
SOX9	AGCACTCGGGGCAATCC	GGAAGTCGATAGGGGGCTGT
CDH1	TCAGCCAATCAGCGGTACG	GAGTCTGAACTGACTTCCGCA
MMP14	GAGCATTCCAGTGACCCCTC	ACCCTGACTCACCCCCATAA
GAPDH	AAGGTCGGAGTCAACGGATTT	TGAAGGGGTCATTGATGGCA

3.3.10. Genome Editing

pHIV-Zsgreen plasmid was kindly provided by Doc. Dr. Şerif Şentürk from İzmir Biomedicine and Genome Center.

Table 18 gRNA used for CRISPR-Cas9 HDR experiment in this thesis

Oligo name	**Sequence**

CTNNB1-gRNA	TTCTAATACGACTCACTATAGTTGCCTTTACCACTCAGAGAGT TTTAGAGCTAGA
CTNNB1-HDR	AGTCACTGGCAGCAACAGTCTTACCTGGACTCTGGAATCCAT TCTGGCGCCACTACCACAGCTCCTTTTTTGAGTGGTAAAGGC AATCCTGAGGAAGAG
KRAS-gRNA	TTCTAATACGACTCACTATAGTAGTTGGAGCTGGTGGCGTGT TTTAGAGCTAGA
KRAS-HDR	CTGAATTAGCTGTATCGTCAAGGCACTCTTGCCTACTCCATC AGCTCCAACCACCACAAGTTTATATTCAG
ARID1A-gRNA	TTCTAATACGACTCACTATAGCAACAAAGTGGAGTGGTGGTG TTTTAGAGCTAGA
ARID1A-HDR	GTGTTTTCCCGGAGCATCTCCAAGCAGTCCTACCACCATTCG ACCTTGTTGCAGCTCACCCCTTGGTCCTGTTCCTCCTCCTTT TCATAAGTTAGTGGTGC
IVT-Scaffold	AAAAAAGCACCGACTCGGTGCCACTTTTTCAAGTTGATAACG GACTAGCCTTATTTTAACTTGCTATTTCTAGCTCTAAAAC

Table 19 Components of Cas9 Nuclease Reaction Buffer (10X, pH=7.9 at 25^{o}C)

Component	**Concentration**
NaCl	1M
MgCl	0.1 M
Tris-HCl	0.5 M
BSA	1mg/ml

Table 20 Components of Cas9 Dilution Buffer

Components	**Concentration**
NaCl	300 mM
Tris-HCl	10 mM
EDTA	0.1 mM
DTT	1 mM

BSA	500 µg/ml
Glycerol	50%

Table 21 Enzymes used for Gene Editing experiments in this thesis.

Enzyme	**Company**	**Catalog no**
Alt-R™ S.p. HiFi Cas9 Nuclease V3, 100 µg	IDT	# 1081060
NotI-HF	New England Biolab	# R3189S
XbaI	New England Biolab	# R0145S
EcoRI-HF	New England Biolab	# R3101S

Table 22 Oligos design for generate overexpression plasmids for this thesis

Oligo name	**Sequence**
CTNNB1-main-Forward	ATATATAGCGGCCGCCACCATGGCTACTCAAG
CTNNB1-main-Reverse	GCGCGCGACTCTAGATTACAGGTCAGTA
CTNNB1-mutasyon-Foward	CTACCACAGCTCCTTTTCTGAGTGGTAAAGG
CTNNB1-mutasyon-Reverse	CCTTTACCACTCAGAAAAGGAGCTGTGGTAG
ARID1A-main-F-2	ATATATATGAATTCGGCTAGCCTCGAGCCACCATGGCCGC
ARID1A-main-R-2	GAGTCTCTAGAATCTCCAAGCAGTCCTACCACCACTCCA

Table 23 Plasmids used for overexpression cloning.

Plasmid name	**Company**	**Catalog No**
pCI-neo beta catenin WT	Addgene	#16518
pcDNA6-ARID1A	Addgene	#39311
PHAGE-KRAS-G12D	Addgene	#116423

pHIV-Zsgreen	Addgene	#18121
psPAX2	Addgene	#12260
pMD2.G	Addgene	#12259

Table 24 Components of FACS buffer

Component	**Amount**
1X PBS	250 ml
%1 BSA	2.5 g
%0.25 Na-Azide	0.05 g
1nM EDTA	1 ml

3.4. Experiments

3.4.1. Cell lines and cell culture

All the cell lines used in this thesis were maintained as 37 °C with 95% humidity and 5% CO2 incubator. T24 and HEK293T cell lines were maintained using the Dulbecco's Modified Eagle Medium (DMEM) supplemented with 10% Fetal Bovine Serum (FBS) and 1% Penicillin. On the other hand, SVHUC-1 and 5637 cell lines were maintained using the RPMI-1640 Medium supplemented with 10% Fetal Bovine Serum (FBS) and 1% Penicillin.

.

3.4.2. Induction Based Neuroendocrine Differentiation

3.4.2.1. EGF Treatment

T24 and 5637 cell lines are treated with 10 ng/ml Recombinant Human EGF, and 2%FBS contained medium. Every 2 day, EGF contained fresh medium or regular medium was added.

3.4.2.2. RNA and protein isolation

3 days after the treatment, RNA and protein were isolated. For RNA isolation, cells were seeded 6 cm plate. 3 days of post treatment, medium was discarded. Cells were washed with 1X PBS. Cells were collected using TrypLE. Then the collected cells were centrifuged at 1500 rpm for 4 minutes, and the supernatant was discarded. RNA was isolated with Monarch Total RNA Miniprep Kit. Concentration of RNA was measured by Nanodrop. RNA was stored at -80°C until further use.

For protein isolation, cells were seeded 10 cm plate. 3 days of post treatment, medium was discarded. Cells were washed with 1X PBS. Cells were collected using TrypLE. Then the collected cells were centrifuged at 1500 rpm for 4 minutes, and the supernatant was discarded. Pellet was dissolved with 150 µl RIPA contained with protease inhibitor cocktail (PIC) lysis buffer. After that, cells were vortexed every 10 minutes for three times and during this time cells were incubated on ice. Lysed cells were centrifuged at max speed at +4°C for 20 minutes. Protein containing supernatant was collected to another Eppendorf and pellet was discarded. Proteins were stored at -80°C until further use.

3.4.2.3. cDNA conversion

To convert RNA to cDNA Thermo Scientific Maxima First Strand cDNA Synthesis Kit for RT-qPCR kit was used according to its protocol. For each reaction 4 µl 5X Reaction Mix and 2µl Maxima Enzyme Mix and 1 µg RNA was added to PCR tube and volume was completed to 50 µl with PCR grade water. Mixture was incubated for 10 min at 25°C followed by 15 min at 50°C.

3.4.2.4. IF staining

Before seeding the cells, the sample number of coverslips were placed in the wells of the 24-well plate. 25 000 cells for T24 cell line and 40 000 cells for 5637 cell line were seeded in 500 µl medium. 3 days after the treatment, cells were removed from the incubator and medium was discarded. Cells were washed 2 times with 250 µl 1X

PBS. Cells were fixed with 250 µl of 4% formaldehyde (in 1X PBS) for 15 min at room temperature on a shaker at 20 rpm. After that cells were washed 2 times with 250 µl 1X PBS. 250 µl of 0.2% TritonX (in 1X PBS) were added, and the pores of the cells were opened on the shaker at room temperature for 45 min. Cells were washed 2 times with 250 µl 1X PBS. 250 µl of 2% goat serum (in 1X PBS) was used to block the cells on a shaker at room temperature for 45 min. Goat serum were discarded and cells were washed with 1X PBS. 80 µl drop of primary antibody diluted according to IF protocol in 2% Goat serum was placed on parafilm. The coverslips were removed with the help of a syringe needle. Inverted and carefully placed on the primary antibody. The parafilms were placed in a box. Cells were incubated 4ºC overnight. Coverslips were inverted again (with the cell surface on top) and placed on a 24 well plate. Cells were washed 2 times with 250 µl 1X PBS. 20 ul Secondary antibody Alexa 594 rabbit (1/500 in goat 2% serum) + DAPI (fc. 300nM) was added top of the cells and they were incubated on a shaker for 2 hours at room temperature. Antibody was discarded and cells were washed with 1X PBS 2 times. Slides were prepared to receive 2 coverslips each. 1 drop of mounting medium was added to 2 ends. The coverslips were inverted and covered with mounting medium on the slides. They were fixed with nail polish and allowed to dry at room temperature. Then they were kept at +4ºC until they were visualized. Images were taken from immunofluorescence microscope and analysis done with ImageJ. Intensity density values was used for analysis.

3.4.2.5. BCA Assay and WB

To measure protein concentration, Pierce™ BCA Protein Assay Kit's protocol was performed. Protein standards were diluted serially six times with RIPA buffer (1000 ug, 500 ug,250 ug, 125 ug,62,5 ug and 31,25 ug). All samples and standards were triplicated. 2 µl protein was added to the each well on 50 µl reagent mix in 96-well plate. To protection against light, plate was folded with aluminum folio and incubated at 37°C for 30 minutes. Lastly, plate was read with Multiskan GO microplate spectrophotometer and protein concentrations were measured.

For 1.5 mm glasses 10 ml Separating gel was prepared for Western Blot. Concentration of gel was determined according to size of the protein. For 10 ml %8 separating gel; 2.7 ml Protogel, 1.25 ml Main gel buffer, 5.05 ml ddH2O, 50 µl %10 APS and 10 µl TEMED were mixed in a 15 ml tube and immediately loaded between the 1.5 ml glasses. To flatten the gel line and prevent bubbles, 1 ml %60 isopropanol was added to the top of separating gel. Gel was incubated for 15-20 minutes for solidify. After that, isopropanol was discarded, and gel was washed gently with water. For 4 ml stacking gel; 0.5 ml Protogel, 1 ml Protogel stacking buffer, 2.5 ml ddH2O, 25 µl %10 APS and 5 µl TEMED were mixed in a 15 ml tube and loaded on frozen separating gel. Comb was placed above stacking gel. Gel was incubated. After the gel was frozen, comb was discarded, and wells were washed with water to get rid of the bubbles.

Glasses were fixed to the PAGE device into the tank. Running Buffer was added up to the indicated point according to gel number. Protein samples and marker were loaded to the wells. Voltage was set to 90 V run for 30 minutes and then raised to 120 V run for 1.5 hours.

To transfer, gel containing glasses were opened in distilled water. Stacking gel part was cut and discarded to waste. 2 sponges and filter papers were wet in 1X transfer buffer. Transfer sandwich was prepared as follows, black side of the cassette, sponge, filter paper, gel, membrane, filter paper, sponge, white side of the cassette. Tank was placed inside a big washbowl and magnetic stirrer was put inside and run. Cassette was placed inside the tank and lid was closed. PAGE device was run at 350mA and for 1.5 hours.

When transfer was done, membrane was blocked with %5 milk powder for 1 hour in room temperature on shaker at 20 rpm. Then milk powder was discarded, and membrane was washed with TBST 3 times on shaker at 50 rpm for 10 minutes. Antibodies were diluted according to datasheet and poured to the membrane and incubated overnight on shaker at 4°C 20 rpm. After the incubation was done, antibodies were collected, and membrane was washed with TBST 3 times on shaker at 50 rpm for 10 minutes. Secondary antibody was diluted according to datasheet and poured on the membrane and incubated at 20 rpm for 1 hour in room temperature. After the

incubation antibody was collected and membrane was washed with TBST 3 times on shaker at 50 rpm for 10 minutes. Membrane was imaged on the Li-COR device.

3.4.2.6. qRT-PCR

To analyze the gene expression at mRNA level, qRT-PCR was done. Neuronal and epithelial to mesenchymal transition genes, WNT pathway genes were determined. FastStart Essential DNA Green Master Kit protocol was followed. cDNA was diluted 1:10. For each reaction, 5 µl FastStart Essential DNA Green Master, 2 µl PCR grade water, 0.5 µl of each primer, 2 µl DNA were mixed. Applied Biosystems 7500 Fast realtime PCR system was used for reading qPCR 96-well plates. Real-time PCR conditions were as follows. Initial denaturation at 95°C for 10 minutes, 40 cycles of denaturation at 95°C for 10 seconds, annealing at 60°C for 20 seconds and extension at 72°C for 30 seconds, final extension at 68°C for 5 minutes. For melting step, 95°C for 10 seconds, 65°C for 60 seconds and 97°C for 1 second.

3.4.2.7. WNT reporter assay

To perform WNT reporter assay, T24 and 5637 cell lines were seeded at 6 cm plate to reach 70-80% confluency the next day. Then transfection was applied according to the Lipofectamine 3000 protocol. In one eppendorf tube, 250 µl OPTIMEM, 4.5 µg pGL3.BAR or pGL3-Basic plasmids, 0.5 µg pGL4.73 [hRluc/SV40] plasmid and 10 µl p3000 was mixed. In another eppendorf tube, 500 µl OPTIMEM and 5 µl Lipofectamine 3000 were mixed. Then,2 eppendorf tubes were mixed and incubated for 15 minutes at room temperature. After the incubation 500 µl of mixture was dropped on T24 and 5637 cells. Next day, each plate was divided into 6 and seeded on 24 well plate. For each triplicate treated with EGF or without treatment. 24 hours later Luciferase reporter assay was applied. For each well, 50 µl Dual-Glo® Reagent was mixed with 50 µl 1X PBS and dropped into the wells. This reagent causes the detachment of cells. Cells were collected and transferred to the 96 well plate. After 45 minutes of incubation, firefly luminescence was measured with MultiskanGo device. Then, 50 µl of Dual-Glo® Stop & Glo® Reagent was added to the wells and incubated for 45 minutes. After 45 minutes of incubation, Renilla luminescence was measured with MultiskanGo device.

Ratio of Luciferase luminescence to renilla luminescence was measured for both pGL3-Basic and pGL3-BAR. Then TCF7/LEF1 contained pGL3-BAR ratio was normalized to the pGL3-Basic control value. Analysis was performed with GraphPad.

3.4.2.8. MTT assay

To perform MTT assay, for T24 cell line 1500 cell and for 5637 cell line 2000 cell seeded in 96 well plate as triplicate and started EGF treatment. 2nd day of the treatment, medium was refreshed. At day 3 of treatment, 10 µl MTT was added to all wells and incubated 4 hours at cell culture incubator. After 4 hours 100 µl solubilization buffer was added to the wells and incubated overnight at cell culture incubator. After incubation, 96-well plate wells were measured at 570nm wavelength with Microplate Spectrophotometer and analyze the values to compare proliferation rate.

3.4.2.9. Colony formation assay

To perform colony formation assay, 500 cell were seeded both 5637 and T24 cells as triplicates to 6-well plate and EGF treatment was started. Every 2 day, medium was refreshed. At day 12, cells were fixed with %3.7 formaldehyde for 20 minutes at RT. Then crystal violet solution (%10 ethanol, %0.1 crystal violet) was added on the cells and incubated for 40 minutes at room temperature. Cells were washed under stream of water. Plate was incubated overnight upside down to discard all water. Finally, plate was scanned with Li-COR device and then images were analyzed with ImageJ program.

3.4.2.10. Wound healing assay

To perform wound healing assay, firstly, 2 parallel lines were drawn with a pencil under the 6-well plate. Cells were seeded as duplicate to a 6-well plate as to be confluent the day 3 of EGF treatment.450 000 cell was seeded. 2nd day of treatment medium was refreshed. 3rd day of the treatment, from top to bottom in a straight line using a 1000ul tip was gently scraped and image was taken form phase contrast microscopy. These images were 0h images. After 10 hour 5637 images and after 18

hour T24 images were taken from phase contrast microscopy again. Images were analyzed with ImageJ program.

3.4.2.11. Spheroid formation assay

To perform spheroid assay formation, first T24 and 5637 cells were collected and counting. Cell number was calculated for every drop should contain 2000 cells/20 ul. Lid were removed from a 10 cm culture dish and add 10 ml of PBS in the dish to keep hydrated environment. Lid was inverted and 20 ul suspension that contains 2000 cells were dropped on the lid. Drops were apart from each other to prevent touching. Lid was inverted onto the PBS contained dish. For EGF treatment, cells were in the 2%FBS and 10 ng EGF medium. Cells were incubated for 3 days. After 3 days, the droplets were visualized by Stereo microscope. Images were analyzed with ImageJ program.

3.4.2.12. Cell cycle assay

To perform cell cycle assay, T24 and 5637 cells were seeded to 6 cm plate and treated with EGF. After 3 days of treatment, cells were detached with TrypLE and collected into 15 ml falcon tubes. They were centrifuged at 300 g for 5 minutes. Supernatant was discarded and they were placed on the ice. 1 ml cold PBS was added to cells and mixed very gently. Then 4 ml cold ethanol was added and mixed. Cells were moved to the -20 ^{o}C and incubated overnight for fixation. Next day fixed cells were collected by centrifugation at 1200 rpm for 15 minutes at 4 ^{o}C and they were resuspended in 100 µl PI-solution (50 µg/mL propidium iodide, 0.1mg/ml RNase A and 0.1% TritonX-100 in 1X PBS), and incubated 15 min at 37°C, shaking every 10 min. After the incubation they were centrifugated at 4500 rpm, at 4^{o}C for 7 minutes, fluorescently stained cells were transferred to polystyrene tubes with 100 µl BD flow buffer (or 1X PBS) and analyzed using Flow Cytometer. Cell cycle phases are analyzed using FlowJo software.

3.4.3. Gene Editing Based Neuroendocrine Differentiation

3.4.3.1. CRISPR-Cas9 HDR

3.4.3.1.1. Oligo Design

For CRISP-Cas9 HDR method, for each gene 3 oligos were designed. One for the guide sequence with T7 promoter, one for the universal scaffold sequence and one for the template for Homology Directed Repair (HDR) template. Oligos were designed using https://www.idtdna.com/site/order/designtool/index/HDRDESIGN web tool.

3.4.3.1.2. sgRNA Synthesis

DNA template for sgRNA in vitro transcription through PCR was generated by preparing the reaction mixture in a sterile RNase-free PCR tube. In a PCR tube, 5 µl IVT-SGRNA oligo (10 µM), 5 µl IVT-SCAFFOLD oligo (10 µM), 25 µl Q5 Hot Start 2X Master Mix and 15 µl nuclease free water were added and mixed. PCR conditions were as follows: initial denaturation at 98 °C for 30 seconds, 35 cycles of denaturation at 98°C for 30 seconds, annealing at 67 °C for 30 second and extension at 62°C for 20 seconds, final extension at 72°C for 2 minutes. After PCR reaction was done, PCR products were run on 1.5% TAE Agarose gel at 100 V for 45 minutes to check whether the product can be seen at 127 bp. The products were isolated using PCR clean-up gel extraction kit, and concentration was measured by Nanodrop.

3.4.3.1.3. T7 In Vitro Transcription

To generate RNA from the DNA template HiScribe™ T7 Quick High Yield RNA Synthesis Kit was used. In a PCR tube, 10 µl NTP buffer mix, 1 µg template DNA, 2 µl T7 RNA polymerase mixes were prepared, and the volume was completed to 30 µl with nuclease free water. The mixture incubated 16 hours at 37 ^{o}C. After the incubation, the DNase treatment was performed to remove DNA template. DNase treatment was performed as follows: 20 µl nuclease-free water was added to each 30 µl reaction, followed by 2 µl of DNase I (RNase-free), mixed and incubated for 15 minutes at 37°C.

3.4.3.1.4. RNA purification

RNA Clean & Concentrator-25 kit was used for RNA purification. 2 volumes of RNA Binding Buffer (100 µl) were added to each sample and mixed. 1.5 volumes of ethanol (95-100%) was added (225 µl) and mixed. Then sample was transferred to the ZymoSpin™ IICR Column in a collection tube and centrifugated at 16000 g for 30 second and the flow-through was discarded. 400 µl RNA Prep Buffer was added to the column and centrifuged at 16000 g for 30 seconds and the flow-through was discarded. Then 700 µl RNA Wash Buffer was added to the column and centrifuged at 16000 g for 30 second and the flow-through was discarded. 400 µl RNA Wash Buffer was added to the column and centrifuged at 16000 g for 1 minute. Column was carefully transferred into a RNase-free tube and 50 µl DNase/RNase-Free water was added directly to the column matrix and centrifuged at 16000 g for 30 seconds. Finally, concentration was measured by Nanodrop.

3.4.3.1.5. In Vitro Cas9 Cleavage Assay

To observe the sgRNA and Cas9 cleavage efficiency, in vitro cleavage assay was performed. 3 µl Cas9 nuclease reaction buffer, 600 nM sgRNA, 1 µM Cas9, 30 nM substrate template were mixed and completed to 30 µl with nuclease free water. In a PCR tube, all the components except the substrate DNA were mixed and incubated at 37 ^{0}C for 10 minutes. After the incubation, substrate DNA was added and incubated 37 ^{o}C for 2 hours. Once the incubation was done, 1 µl of Proteinase K was added to each sample, mixed, and incubated at room temperature for 10 minutes. Next, the products were run on 1.5 % agarose gel 45 minutes and cleavage efficiency was analyzed.

3.4.3.2. Overexpression of Mutated Genes

3.4.3.2.1. Generation of Plasmid Stocks Obtained from Addgene

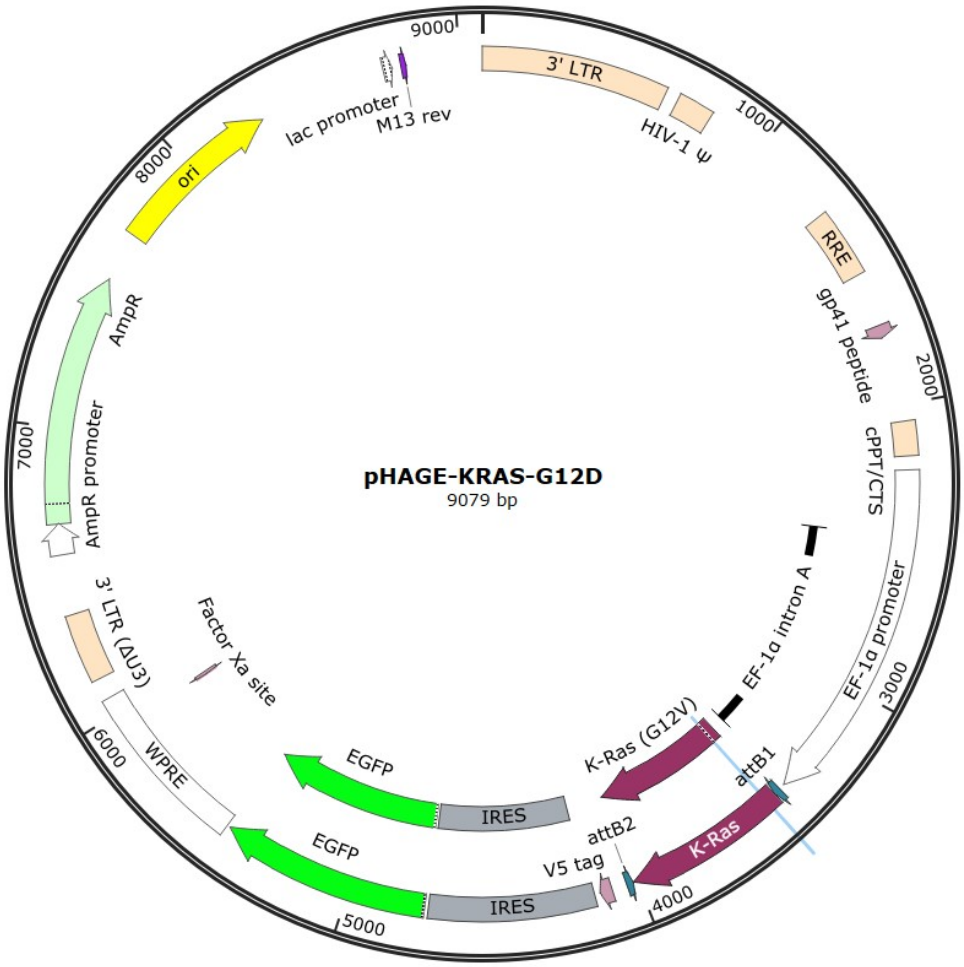
We received the plasmids in bacteria stock from Addgene. For the plasmid isolation first, inoculation loop was sunk into the bacterial stock and spread to the agar

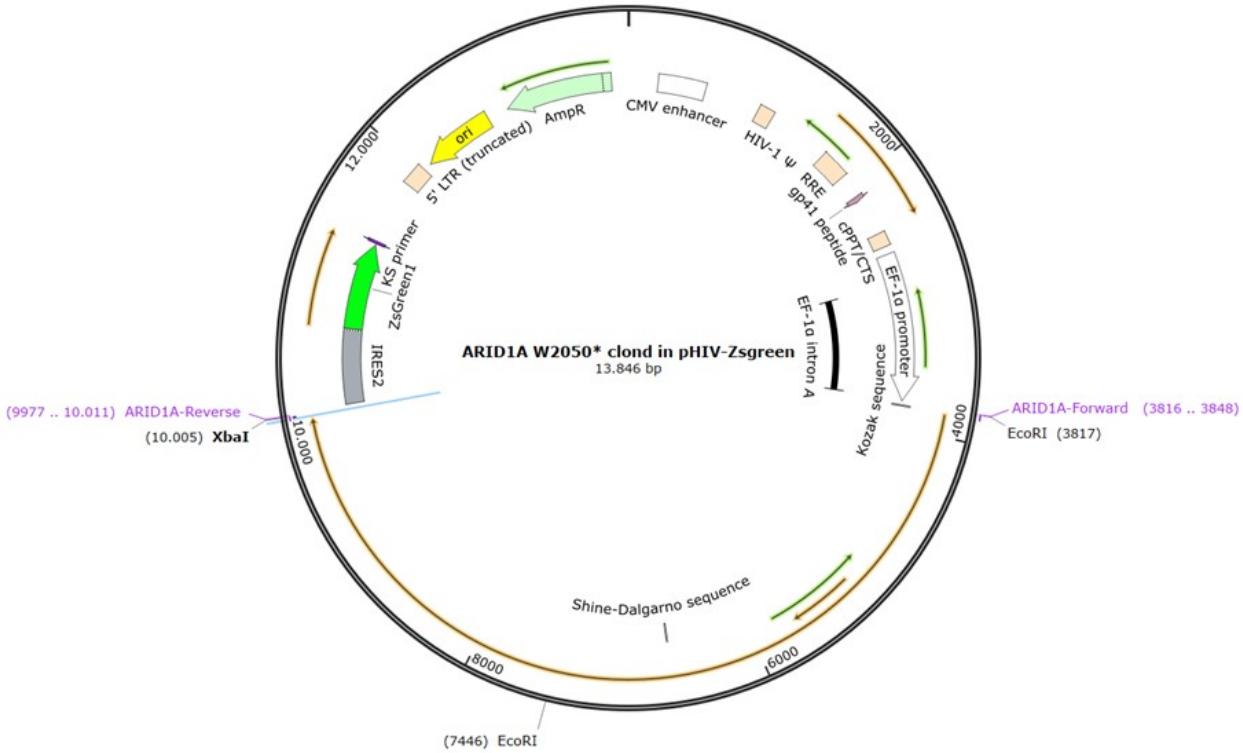
plate. Plates were incubated at 37 ºC overnight. After the incubation, colonies were selected, colonies were grown in 15 µl Ampicillin containing 15 ml LB medium at 37°C on a bacteria shaker (225 rpm) overnight. Plasmid DNA was isolated using Mini Plasmid DNA Purification kit and the concentration was measured with Nanodrop.

3.4.3.2.2. Generation of CTNNB1-S45F, KRAS G12D and ARID1A W2050* Plasmids and Preparation for Lentiviral Transduction

Wild type *CTNNB1* gene was retrieved from pCI-neo beta catenin WT plasmid. Wild type *ARID1A* gene was retrieved from pcDNA6-ARID1A plasmid. Once the PCR is done to generate the mutated version of genes and digestion is performed, pHIVZsgreen plasmid will be used as backbone for lentiviral transduction. For digestion, CTNNB1 plasmid will be digested with NotI and XbaI enzymes and ARID1A will be digested with EcoRI and XbaI enzymes.

KRAS G12D mutated gene was already generated with PHAGE-KRAS-G12D plasmid and available to use for lentiviral transduction.


pHAGE-KRAS-G12D
9079 bp
9000
1000
2000
3000
4000
5000
6000
7000
8000
3' LTR
HIV-1 ψ
RRE
gp41 peptide
cPPT/CTS
EF-1α promoter
EF-1α intron A
attB1
K-Ras
attB2
V5 tag
K-Ras (G12V)
IRES
EGFP
IRES
EGFP
WPRE
3' LTR (ΔU3)
Factor Xa site
AmpR promoter
AmpR
ori
lac promoter
M13 rev


ARID1A W2050* clond in pHIV-Zsgreen
13.846 bp
2000
4000
6000
8000
10.000
12.000
CMV enhancer
AmpR
ori
5' LTR (truncated)
HIV-1 ψ
RRE
gp41 peptide
cPPT/CTS
EF-1α promoter
Kozak sequence
EF-1α intron A
KS primer
ZsGreen1
IRES2
Shine-Dalgarno sequence
(9977 .. 10.011) ARID1A-Reverse
(10.005) XbaI
ARID1A-Forward (3816 .. 3848)
EcoRI (3817)
(7446) EcoRI

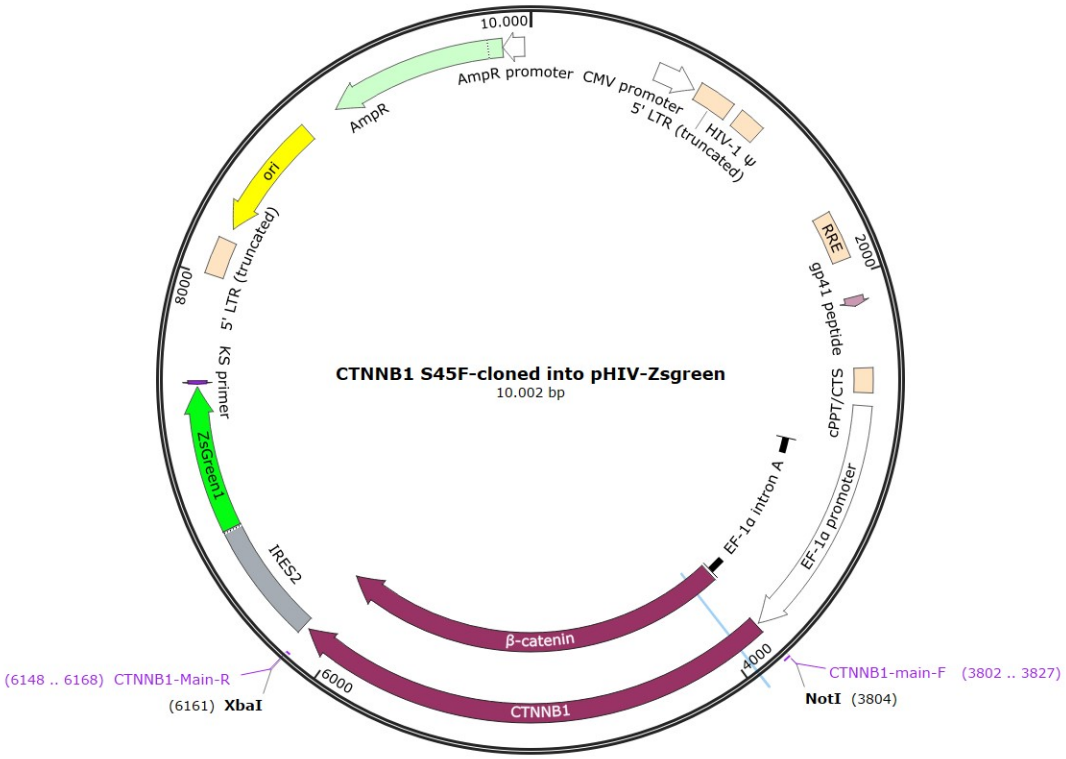


Figure 6 Map of mutant KRAS, ARID1A and CTNNB1 plasmids. Blue lines indicate the mutation points.

3.4.3.2.3. Lentiviral Transduction for PHAGE-KRAS-G12D Plasmid

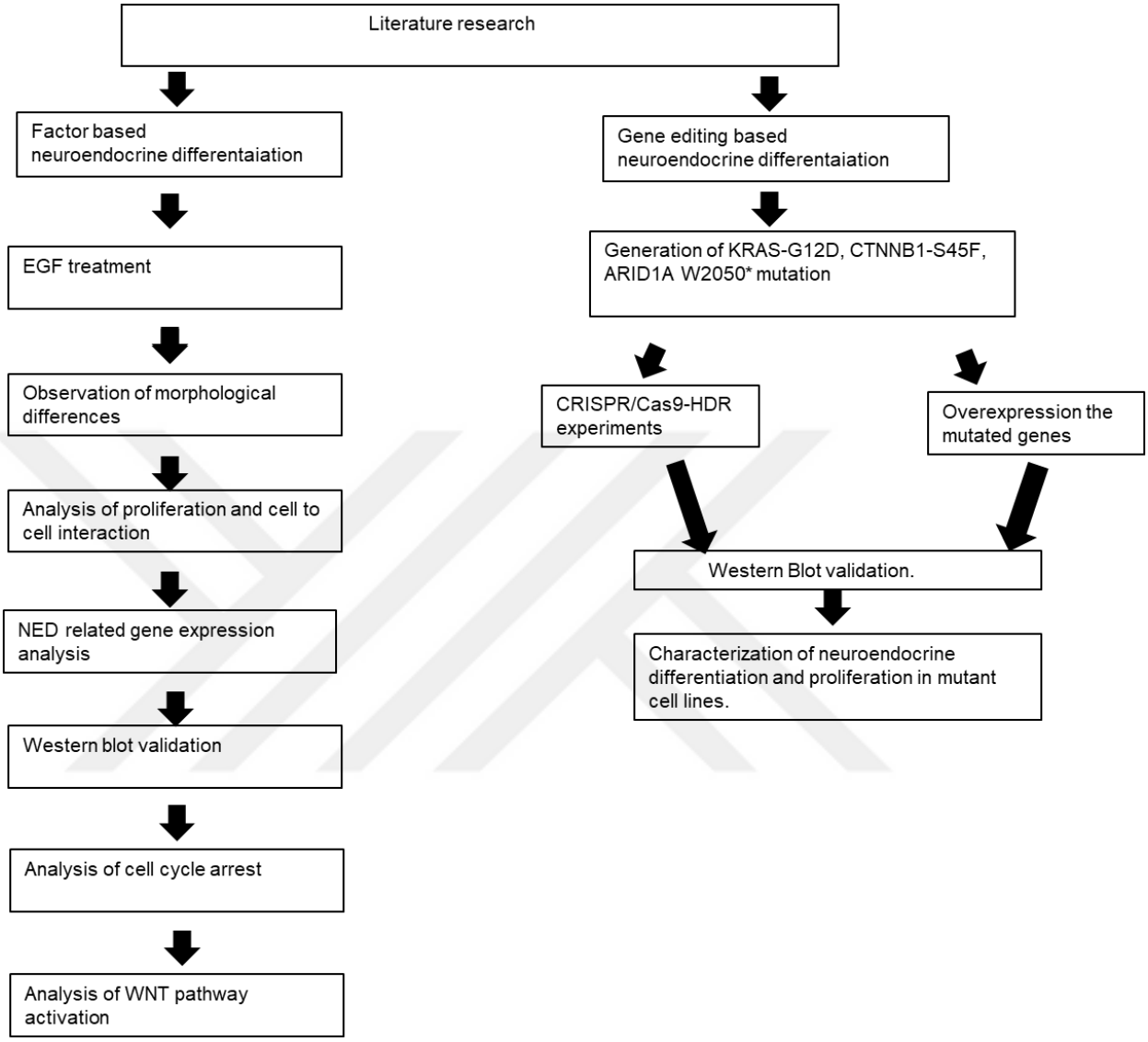
HEK293T cells were transfected with PHAGE-KRAS-G12D and pHIV-Zsgreen plasmids. HEK293T cells were seeded 10cm plate and once the cells reached 80% confluency medium was changed. In regular cell culture laboratory, transfection was applied according to the Lipofectamine 3000 protocol. In one eppendorf tube, 500 µl OPTIMEM, 3µg PHAGE-KRAS-G12D or pHIV-Zsgreen plasmids, 6µg pSPAX2, 3µg pMD2.G plasmid and 24 µl p3000 was mixed. In another eppendorf tube, 500 µl OPTIMEM and 12 µl Lipofectamine 3000 were mixed. 2 eppendorf tube were mixed and incubated for 15 minutes at room temperature. After the incubation 1 ml of mixture was dropped on HEK293T cells. Then cells were moved to Lentivirus laboratory. After 24 hours, medium was collected at 15 ml falcon tube and stored 4^0C. 10 ml of fresh medium was added to HEK293T cells and placed in the incubator. After 24 hours,

medium was collected with a new 15 ml falcon. Viruses collected in falcons were passed through a 0.45µm syringe filter, combined in 50ml Falcon, aliquoted to 1ml into cryo and stored at -80^{0}C freezer. When SV-HUC-1 cells reached 50-60% confluency, medium was removed in regular cell culture laboratory, cells were washed with PBS and 7.6 ml of fresh medium was added. Next cells were transferred to the lentivirus laboratory and the virus aliquot was taken from -80^{0}C on ice. 8µl of 8mg/ml 1000x polybrene stock was added to the plates and the plates were shaken. The virus was rapidly thawed at 37^{0}C and added dropwise to the plates in 400µl (1/20) aliquots. Plates were placed in the incubator. After 24 hours, GFP expression was checked. Plates were washed twice with 12ml PBS, 10ml fresh medium was added and the plate was transferred to regular cell culture laboratory. 72 hours after transduction, cells were prepared for cell sorting. Medium was discarded and cells were washed with 1X PBS and collected using TrypLE. Then the collected cells were centrifuged at 1500 rpm for 4 minutes, and the supernatant was discarded. Pellet was resuspended with 1 ml ice cold FACS Buffer. After that, cells were taken to the BD FACSAria III for sorting. The top %4 GFP positive cells were sorted as single cells on 96-well plates. Remaining GFP positive cells were sorted as bulk.

3.5. Data evaluation

Prism 9.0 (GraphPad, USA) software was used to visualize the data as graph. Welch's Test analysis was used all the comparison. Significance threshold was set as p value < 0.05. Also, all data are given as mean ± S.E.M with *p < 0.05, **p < 0.01 and ****p < 0.0001.

3.6. Study plan



3.7. Ethics committee approval

This study was approved by the Izmir Biomedicine and Genome Center NonInterventional Research Ethics Committee (IBG-GOEK) on 28.01.2022. Ethics committee approval protocol number is 2022-002.

4. RESULTS

4.1. Induction based modeling – EGF Treatment

4.1.1. EGF treatment causes morphological changes.

After 3 days of 10 ng EGF treatment, images of control and treated cells were taken from brightfield microscopy, and some morphological changes were observed. Some of the cells lost their round structure and some cells gained neurite- like extension (thin-long) extensions (Figure 6). They gained morphological characteristics of neuron-like cells. Also, observation showed that their proliferation rate was decreased. Therefore, it was concluded that EGF treatment cause morphological changes on cells.

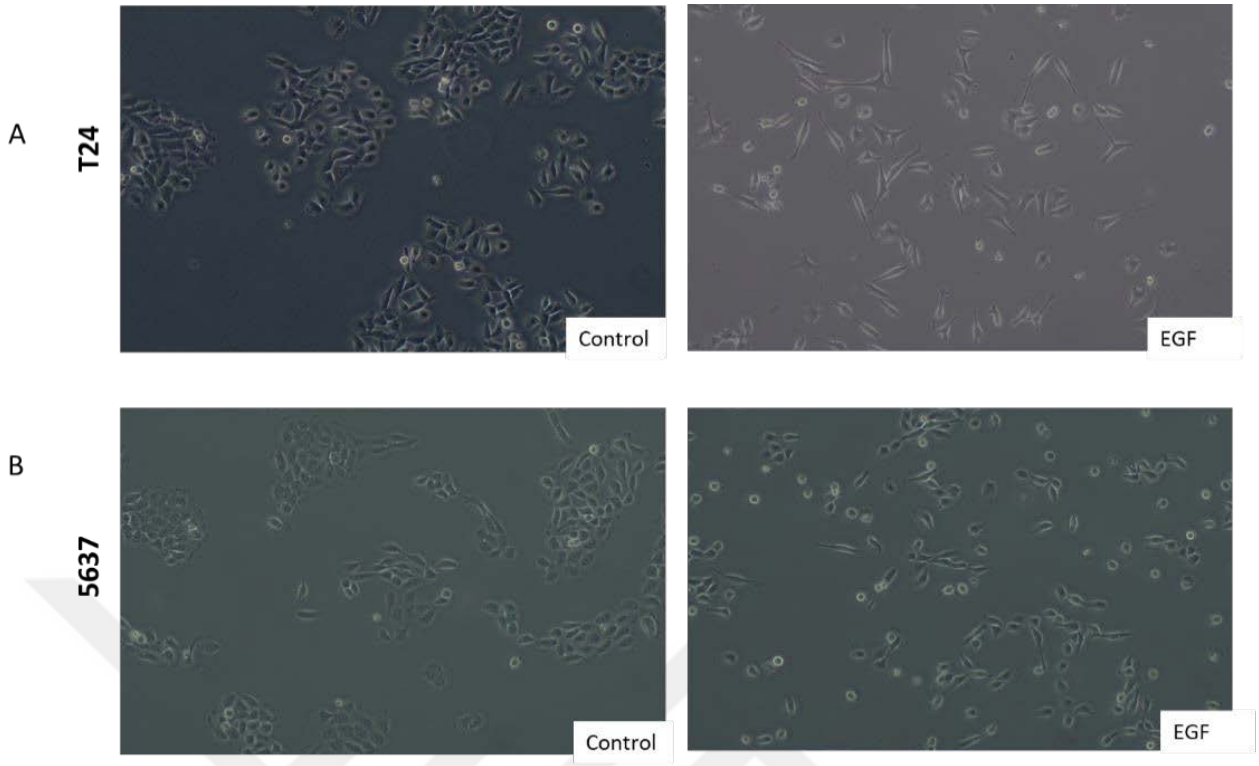
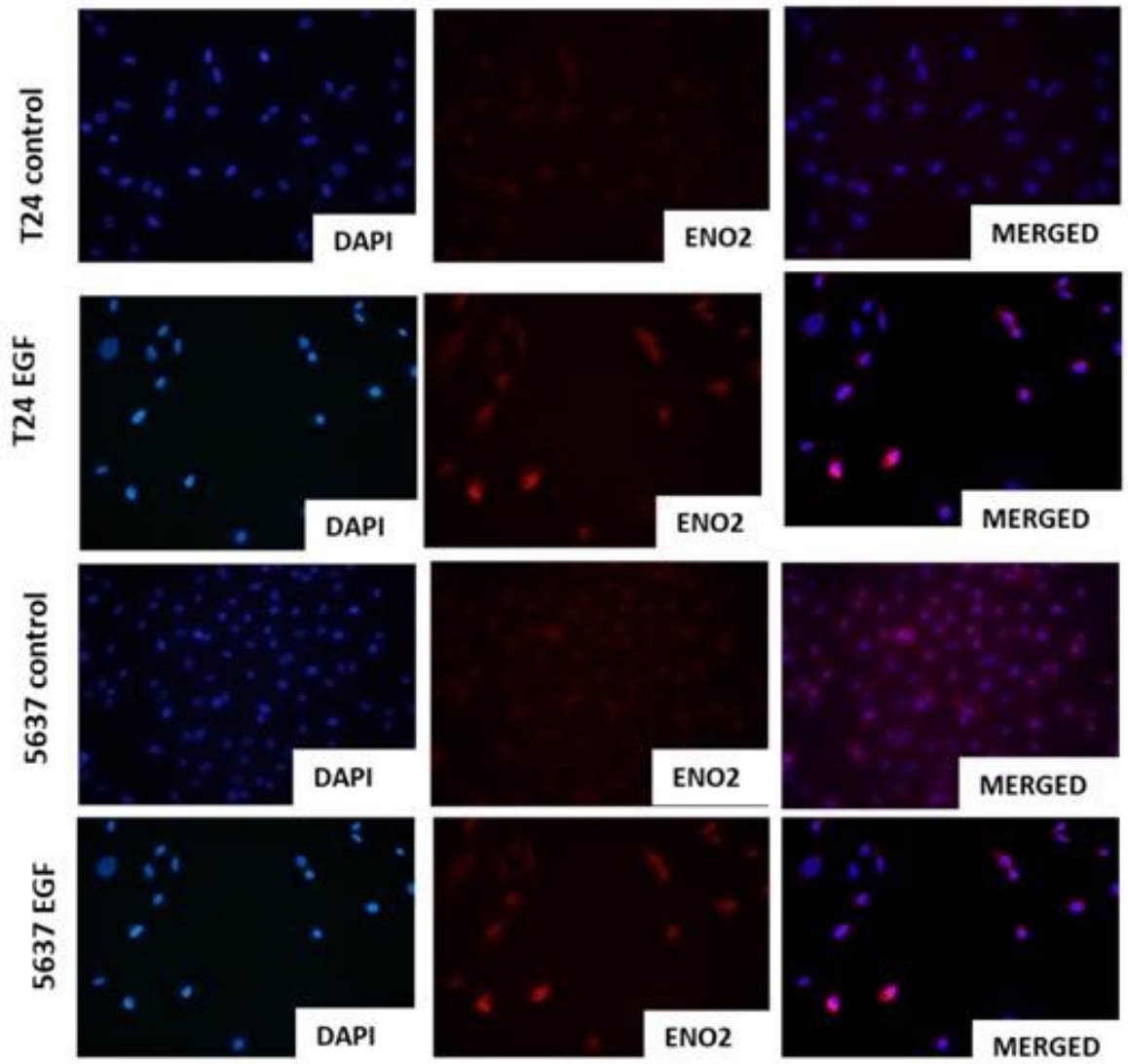
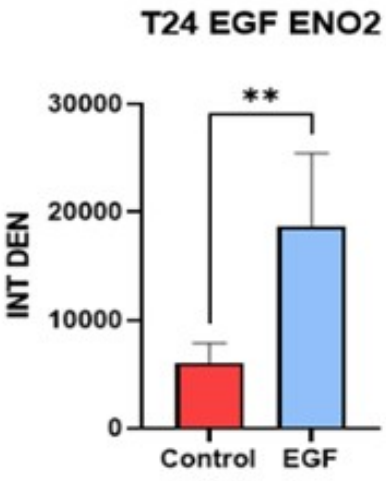


Figure 7 Brightfield images of T24 and 5637 cell lines after 3 days of EGF treatment. A) T24; B) 5637

4.1.2. EGF treatment causes neuroendocrine differentiation.

After 3 days of 10 ng EGF treatment, immunofluorescence staining was performed with ENO2 and ChgA antibodies which are neuroendocrine differentiation markers. Once the staining images were taken, analysis was done with intensity density values. Treated cells showed higher intensity density of the tested markers than control (Figure 7 and Figure 9). For the confirmation of immunofluorescence results, qRT-PCR experiments were performed to see the gene expression changes in *ENO2* and *ChgA*. *ENO2* was upregulated both T24 and 5637 (Figure 8). However, expression of *ChgA* did not show any significant changes (Data not shown). These data shows that EGF treatment results in neuroendocrine differentiation in 5637 and T24 cells.


T24 control
DAPI
ENO2
MERGED
T24 EGF
DAPI
ENO2
MERGED
5637 control
DAPI
ENO2
MERGED
5637 EGF
DAPI
ENO2
MERGED


T24 EGF ENO2
INT DEN
30000
20000
10000
0
**
Control
EGF

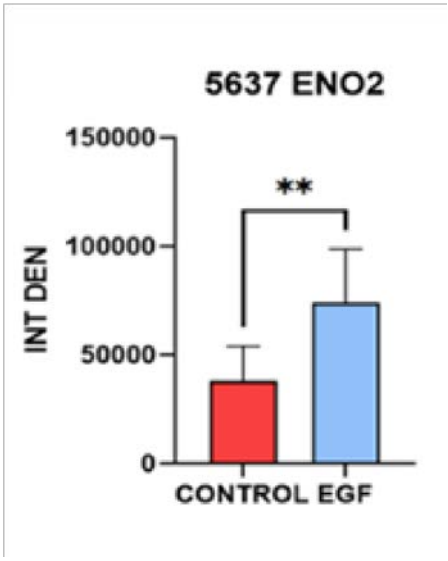

5637 ENO2
INT DEN
150000
100000
50000
0
**
CONTROL EGF

*Figure 8 Immunofluorescence staining images of ENO2 staining (Upper panel) and bar plot which shows intensity density analysis of ENO2 in T24 and 5637 cell lines comparing the EGF treated and control cell lines. (Lower panel). (Welch's t test p value = T24: <0,0001 5637: 0,0012) (*p < 0.05; **p < 0.01; ***p < 0.001)*

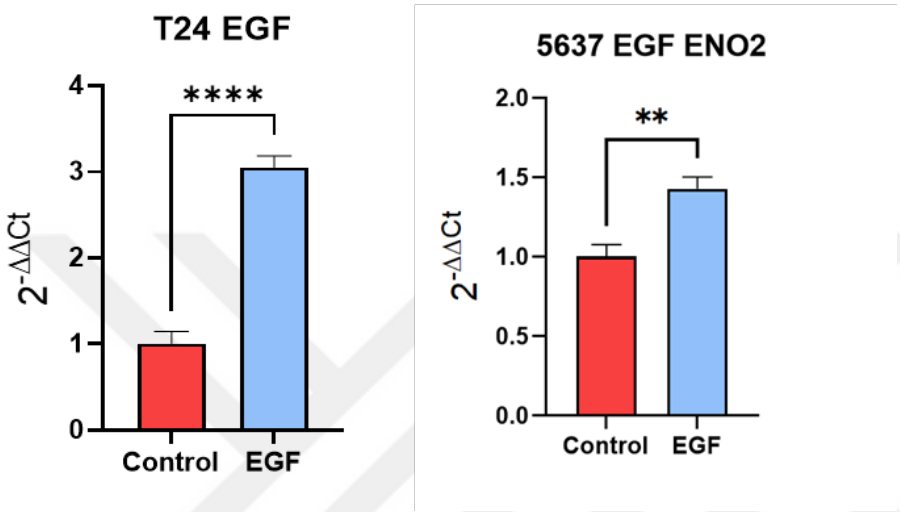


*Figure 9 qRT PCR result of ENO2 expression in T24 (Left panel) and 5637 (Left panel) cells, comparing EGF treated and control cell lines. (Welch's t test p value = T24: 0,0052 5637: 0,0021) (*p < 0.05; **p < 0.01; ***p < 0.001)*

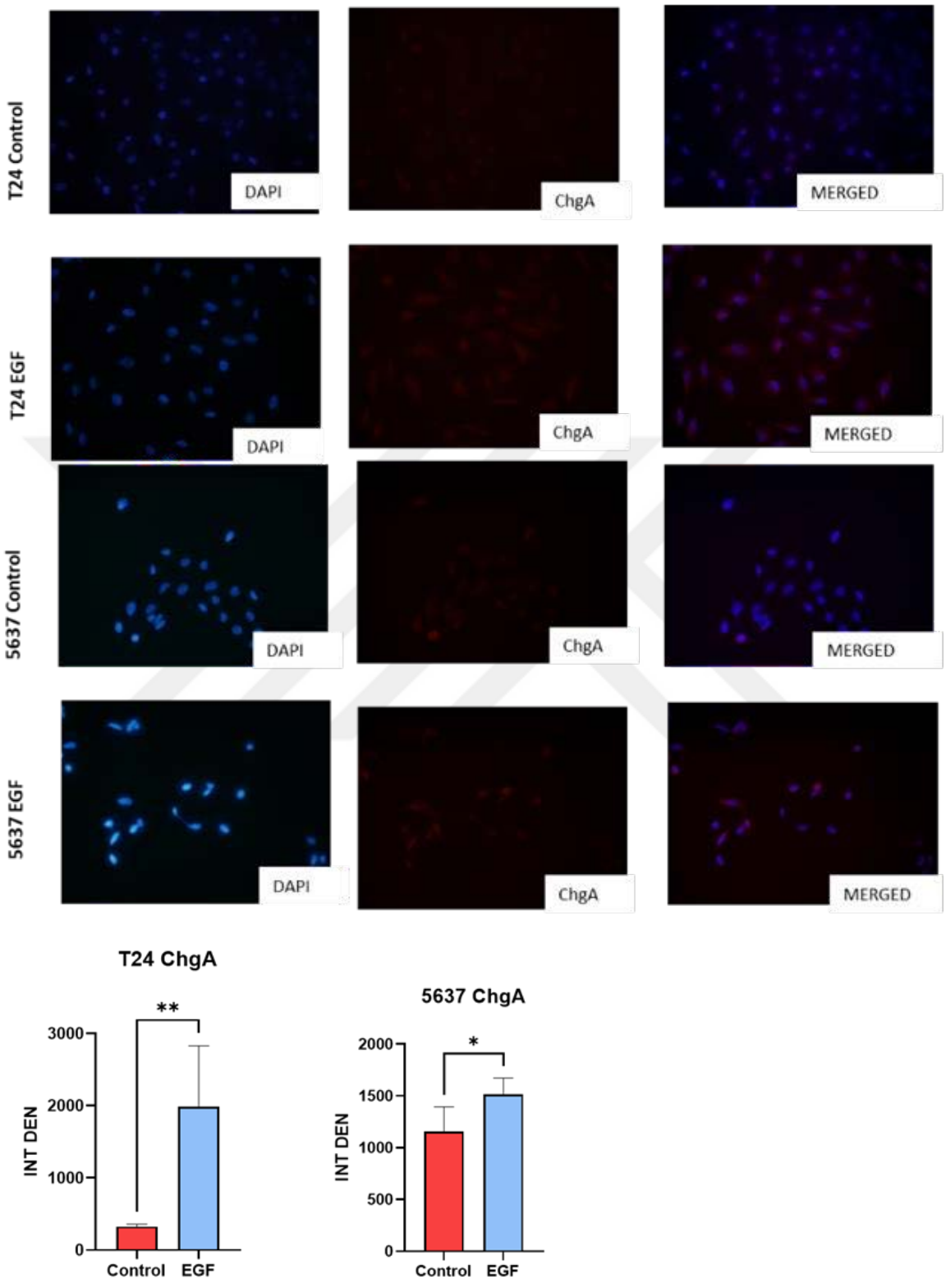


Figure 10 Immunofluorescence staining images of ChgA staining (Upper panel) and bar plot which shows intensity density analysis of ChgA both T24 and 5637 cell lines

*comparing the EGF treated and control cell lines. (Lower panel). (Welch's t test p value = T24: 0,0019 5637: 0,0156) (*p < 0.05; **p < 0.01; ***p < 0.001) (Experiment performed with at least 6 technical replicates)*

4.1.3. EGF treatment affects proliferation, colony formation and spheroid formation.

While culturing the cells after EGF treatment, a decrease in prolifreation rate has been already realizedTo quantitatively evaluate this decrease, MTT assay was performed. The assay was tested using different numbers of cells to detect changes in proliferation rate (not shown). Ultimately 4000 cells and 6000 cells was seeded for T24 and 5637 cells, respectively. MTT assay confirmed the significant decrease in proliferation rate in both cell lines (Figure 10).

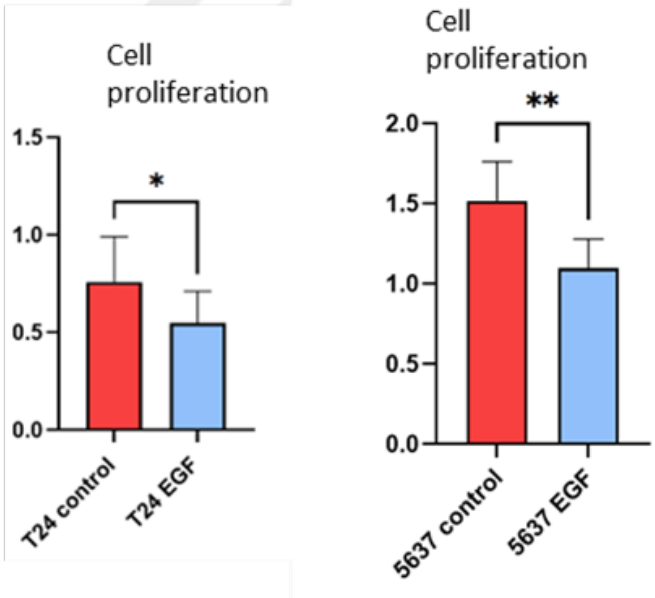


*Figure 11 Cell proliferation analysis. Bar plots represent the MTT proliferation assay results comparing EGF treated and control cells. (Welch's t test p value = T24: 0,0428 5637: 0,0011) (*p < 0.05; **p < 0.01; ***p < 0.001) (Experiment performed with 3 biological and 3 technical replicates)*

Also, it was observed that cell to cell contact was decreased as observed by microscopy. Here, colony formation assay was performed to analyze the colony formation capacity of after EGF treatment .As it can be seen in Figure 11, after 12 days, colony formation ability of 5637 cells was significantly decreased (Left panel). Additionally, it was observed that T24 cell line lost the ability of colony generation completely such that the analysis could not be done with ImageJ (Figure 11).

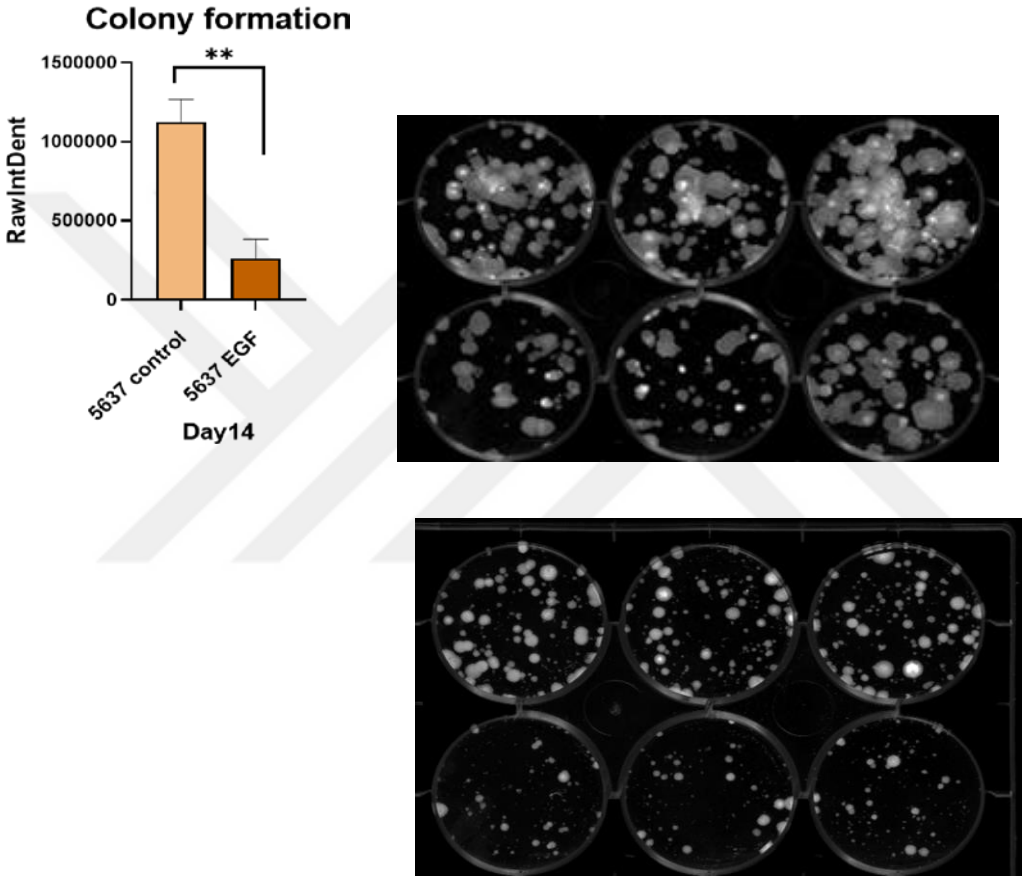


Figure 12 Colony formation images and analysis. Bar plot represents the colony formation signal intensity of 5637 cell line comparing EGF treated and control cells (Left panel). Colony formation plate images of both T24 and 5637 cell lines comparing EGF treated and control cells (Right panel). (Experiment performed with 3 biological and 3 technical replicates)

Then spheroid formation capability was measured by spheroid formation assay. Spheroid areas was measured and EGF treated cells showed decreased spheroid

formation capability in both T24 and 5637 cell lines.The area of spheroids were measured and analyzed by the ImageJ. (Figure 12).

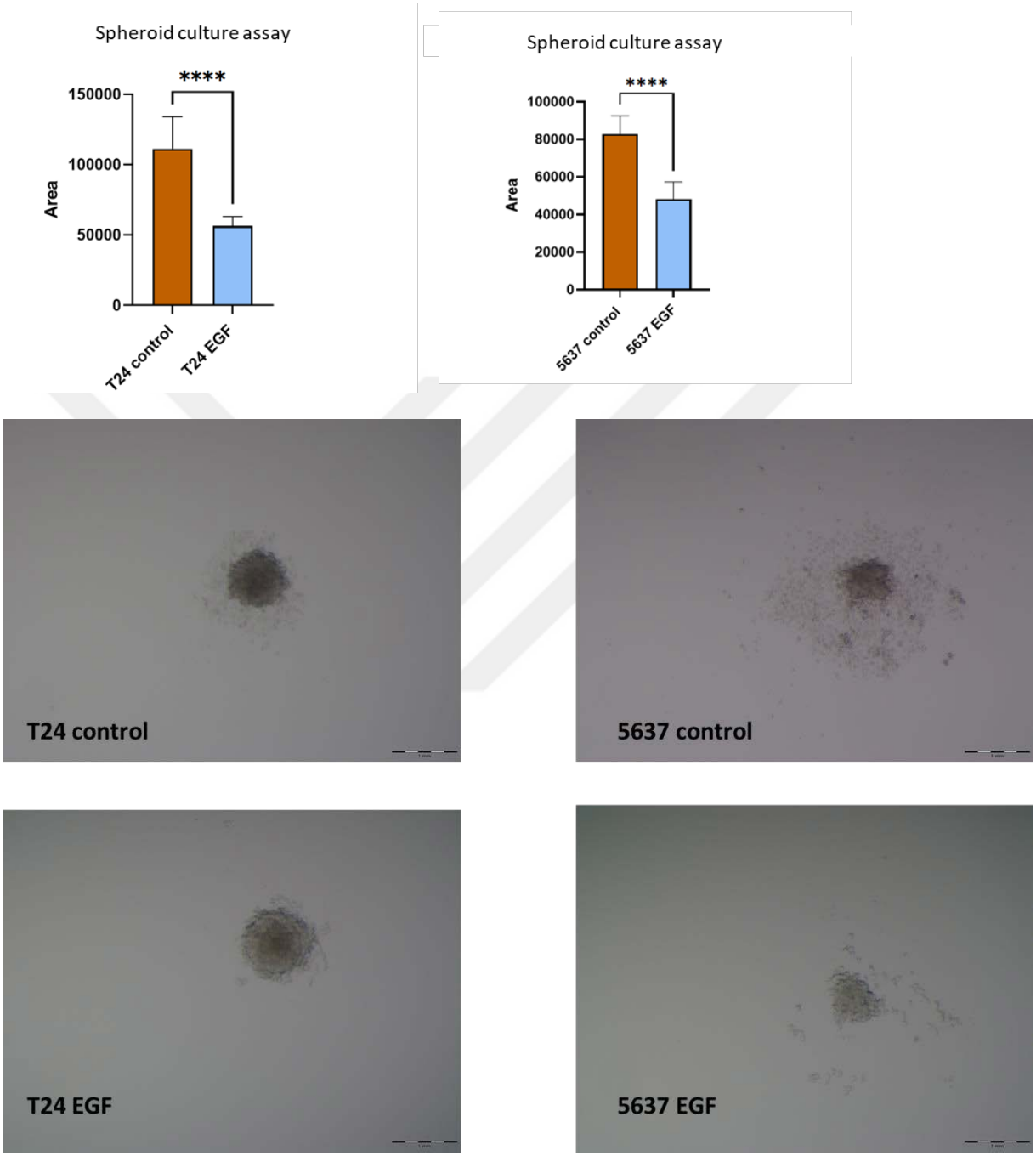


Figure 13 Spheroid formation images and bar plots representing the analysis in both T24 and 5637 cell lines. (Welch's t test p value = T24: <0,0001 5637: <0,0001) (Experiment performed with 2 biological and at least 6 technical replicates)

As a result of all these analysis, it was concluded that EGF treatment affect the cells' proliferation rate, colony fomation and spheriod formation capabilities.

4.1.4. EGF treatment affects the cell invasion capability

To analyze how EGF tretment affect the invasion characteristics, scratch assay was performed both T24 and 5637 cell lines comparing EGF treated and control cell lines. Wound healing percentage was compared betweeen control and EGF treated cells. Although analysis showed opposite changes, EGF treatment affect the invasion characteristics but further analysis and studies should be performed the understand this differences.

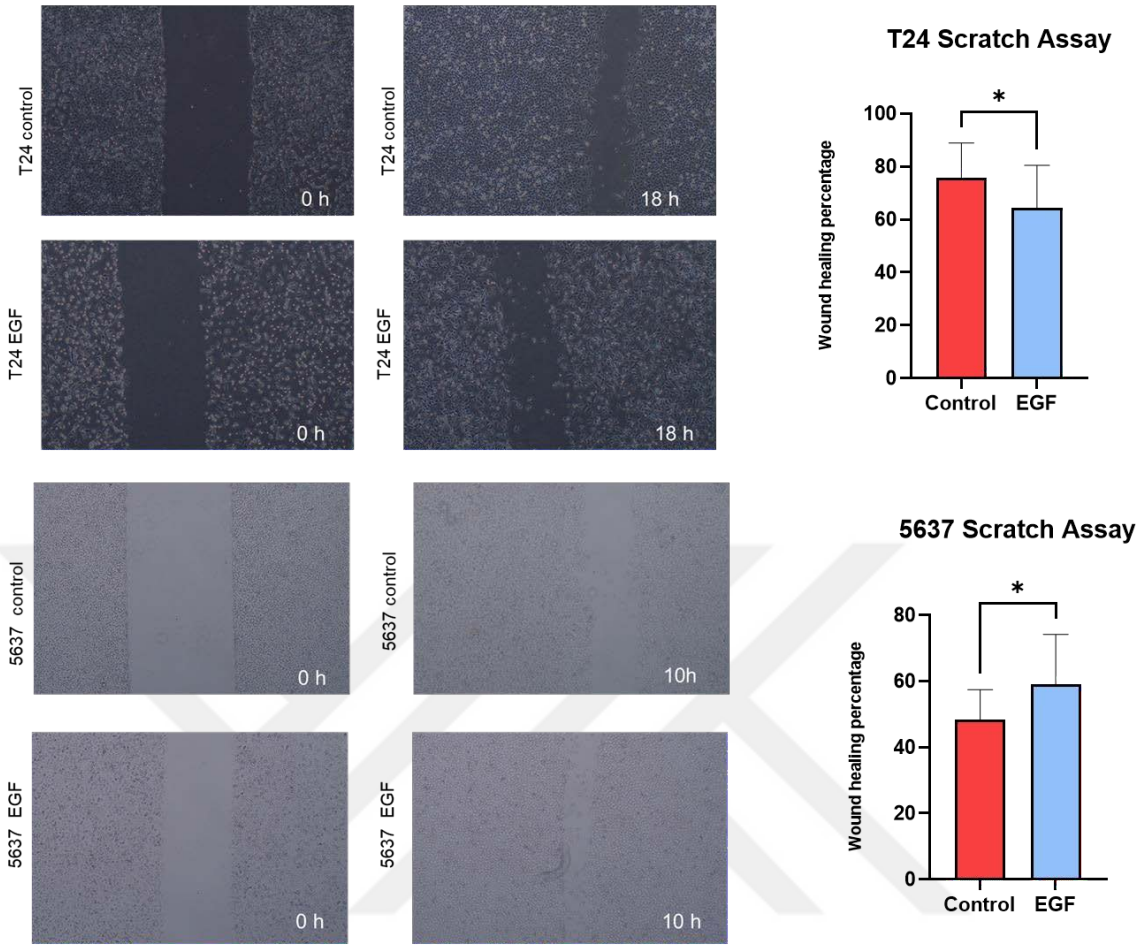


*Figure 14 Scratch assay images and quantitively analysis of T24 (upper panel) and 5637 cell lines (lower panel). (Welch's t test p value = T24: 0.0414 5637:0.0288) (*p < 0.05; **p < 0.01; ***p < 0.001) (Experiment performed with at least 6 technical replicates)*

4.1.5. EGF affects the cell cycle and cause G0/G1 arrest

To observe and analyze how the cell cycle was affected due to EGF treatment, cell cycle analysis was performed. After 3 days of EGF treatment, cells were fixed and stained with PI. Then cells were analyzed with Flow Cytometry. MTT assay showed that the proliferation rate was decreased after EGF treatement (Figure 11) so cell cycle arrest at G0/G1 phase was expected. Indeed 5637 cell line shows this arrest.Percentage of cells in G0/G1 stage was slightly increased (Figure 15). However

in T24 cell line, there was an unexpected decrease in G0/G1 phase, which is a result pending for further analysis and replication. Although there were differences between two cell lines, it could be concluded that EGF treatment affects the cell cycle and causes cell cycle arrest.

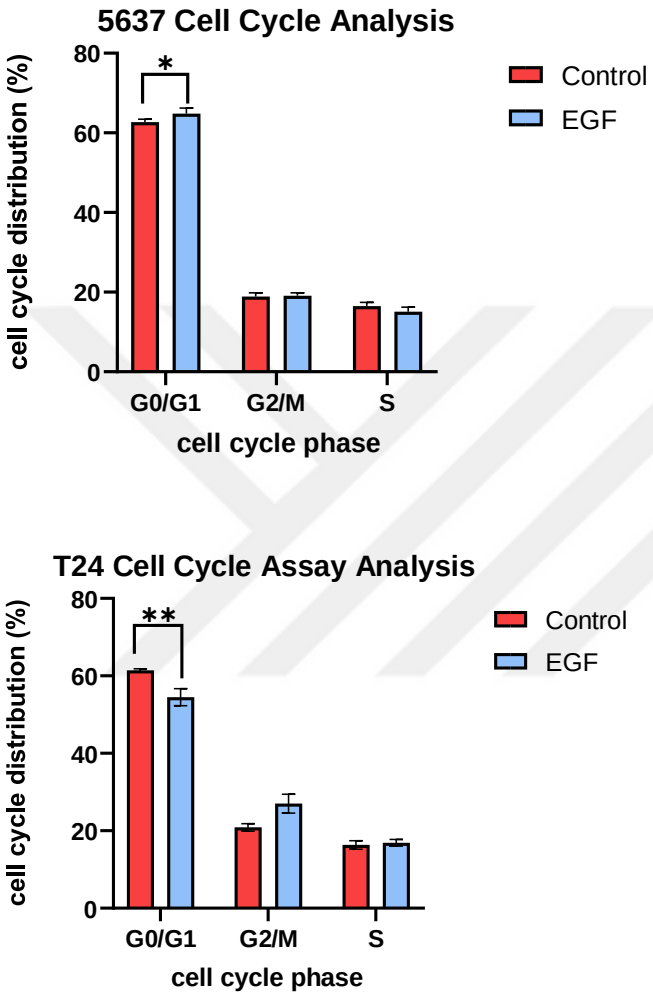
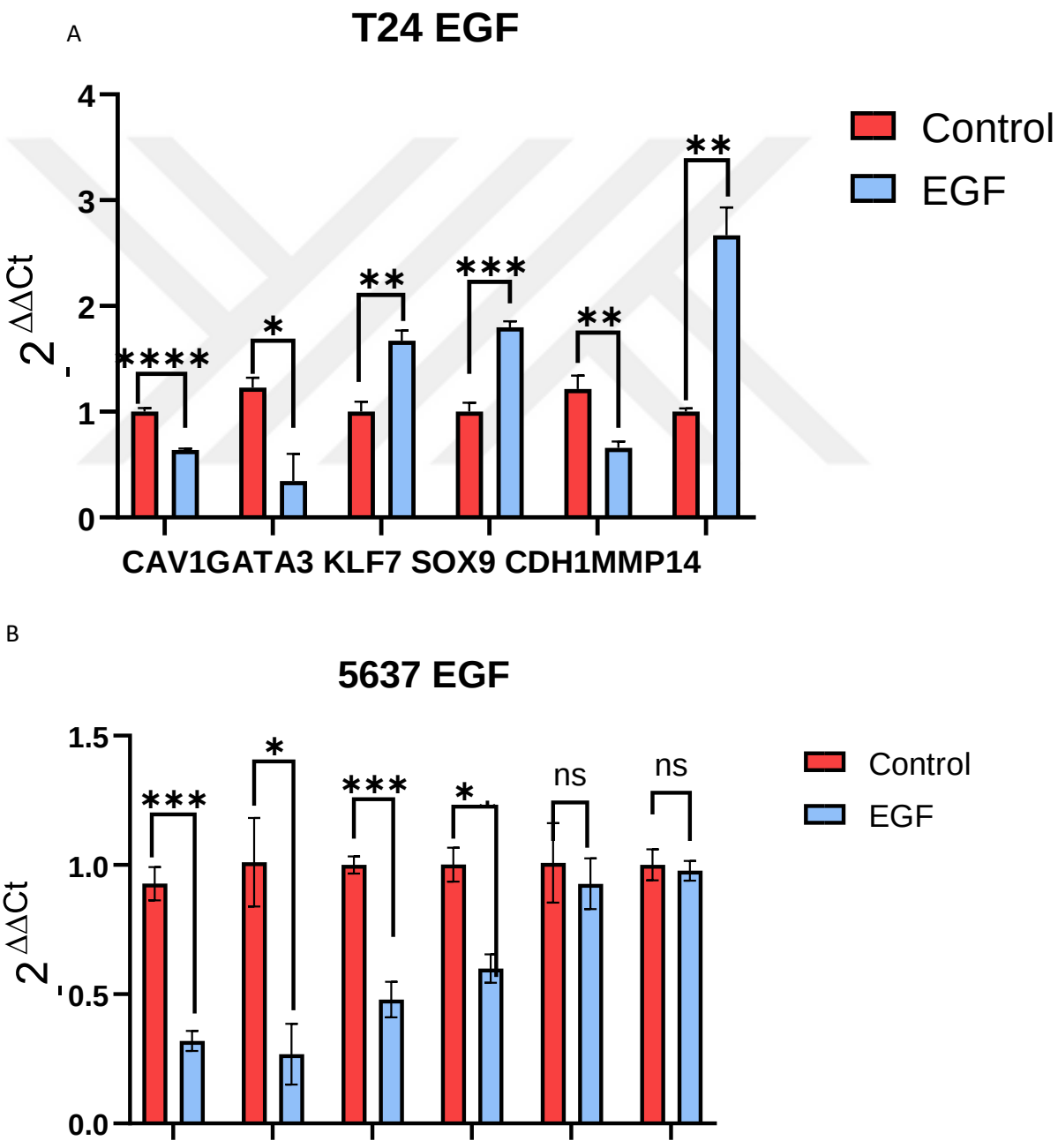


Figure 15 Cell cycle arrest analysis of T24 and 5637 cell line with PI staining, comparing EGF treated and control cell lines. (Experiment performed with 2 biological and 2 technical replicates)

4.1.6. EGF affects the neuroendocrine differentiation related gene expression.

To observe how the expression of gene involved in neuroendocrine differentiation was affected, qRT- PCR was performed in both T24 and 5637 cell lines comparing

EGF treated and control cells (Figure 17). After 3 days of EGF treatment, mRNA was isolated from both control and EGF treated cell lines and converted to cDNA. Then qRT PCR was performed. Expression levels of *CAV1, GATA3, KLF7, SOX9, CDH1, MMP14* genes was analyzed. Although there were some differences in the expression profiles of those genes in T24 and 5637, results showed that EGF treatment affects the expression level of neuroendocrine differentiation related genes.



CAV1 GATA3 KLF7 SOX9 CDH1 MMP14

*Figure 16 q-RT PCR analysis of neuroendocrine differentiation related genes. A) T24 cell line result (Welch's t test p value CAV1: 0,0011 KLF7: 0,0137 SOX9: 0.0003) B)5637 cell line result (Welch's t test p value CAV1: 0,0188 GATA3: 0,0113 KLF7: 0,0016 SOX9: 0,0014 CDH1: 0,4875 MMP14: 0,6648) (*p < 0.05; **p < 0.01; ***p < 0.001) (Experiment performed with 3 biological and 3 technical replicates)*

4.1.7. EGF treatment induces EMT.

It has been known that CDH1 gene is related to epithelial to mesenchymal transition (EMT) and EGF treatment should decrease its expression. In this context, qRT-PCR results (Figure 18) confirmed the downregulation of E-cadherin expression as an mRNA level. For the validation of qRT-PCR result, after 3 days of EGF treatment in both T24 and 5637 cell lines, immunofluorescence staining was performed using the antibody against E-cadherin. Intensity density value was used for analysis. In line with qRT-PCR, E-cadherin staining intensity density was downregulated after EGF treatment compared to the control cells.

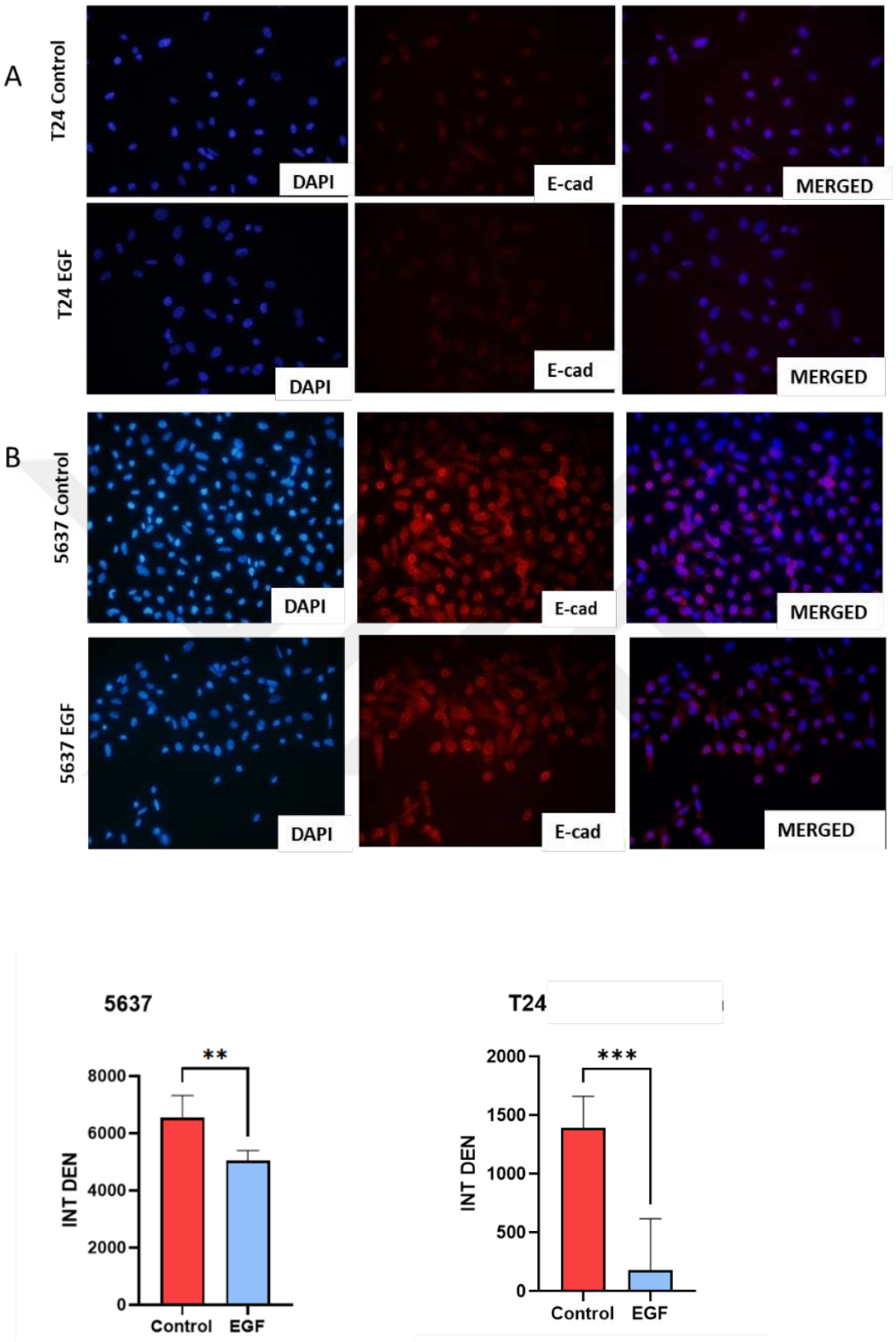
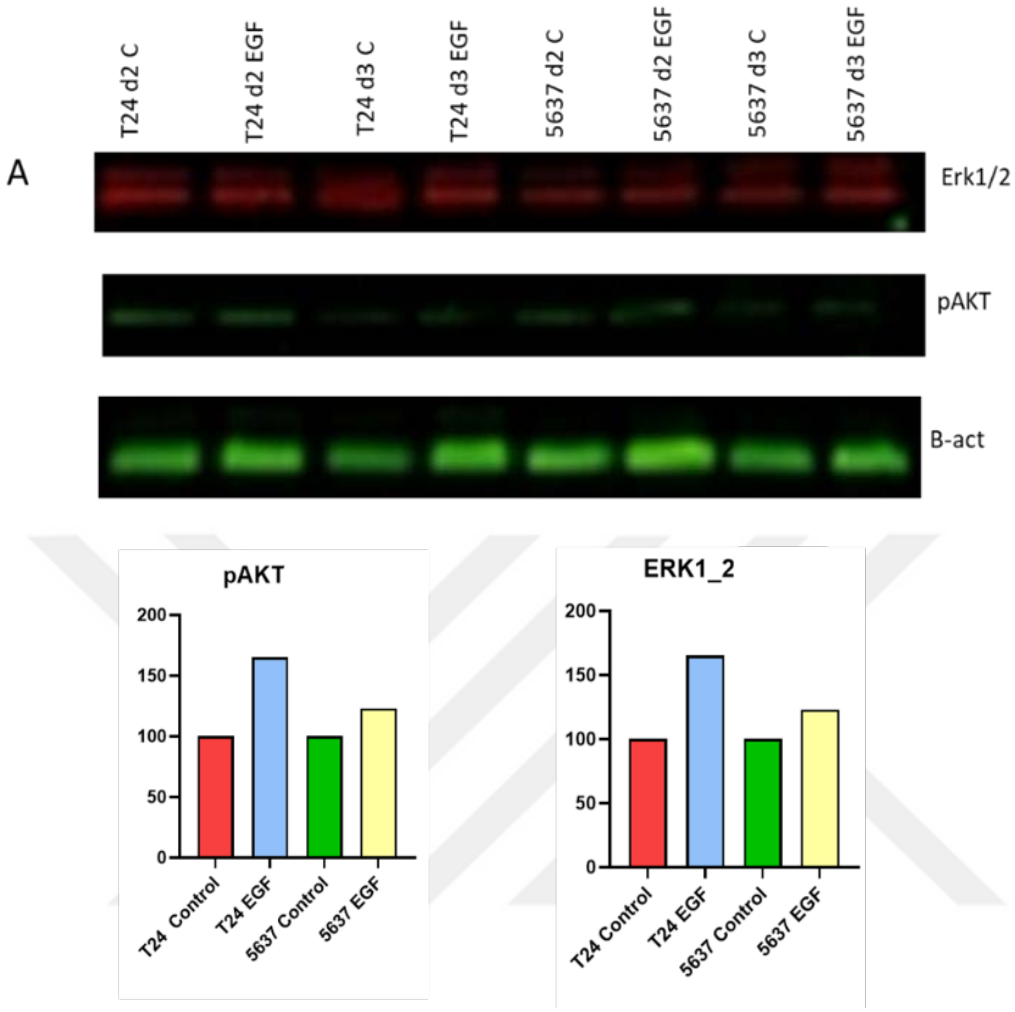


*Figure 17 Immunofluorescence images and analysis of E-cadherin staining (Upper panel) Images of T24 and images of 5637 (Lower panel). Intensity density analysis of E-cadherin expression (Welch's t test p value = T24: 0,0004 5637: 0,0039) (*p < 0.05;*

***p < 0.01; ***p < 0.001) (Experiment performed with at least 6 technical replicates)*

4.1.8. EGF activates Akt-Erk pathway in bladder cancer cells.

It has been known that EGF signaling trigger the activation of Akt/Erk signaling pathway which control the cell proliferation. To analyze whether this pathway was activated, the expression level of some of the proteins involved in this pathway was controlled by Western Blot (Figure 19A). Protein was isolated both 2 days and 3 days after the EGF treatment both T24 and 5637 cell lines to compare the activity in control and EGF treated cells. However, the analysis was done only for the 3 day treated samples. The results showed that activation of Erk1/2 and pAKT was more apparent in T24 cell line compared to 5637 cells Also, the expression level of MAP4K4 (Figure 19B) which is one of the mediators of Akt/Erk pathway(Gao et al., 2017), was analyzed by qRT-PCR. In this case, although the expression of MAP4K4 was significantly upregulated in T24 cell line, for 5637 cell line it was significantly downregulated. This discrepancy needs further investigation. However, overall, the results showed that EGF treatment most likely induces the Akt/Erk pathway.


A
T24 d2 C
T24 d2 EGF
T24 d3 C
T24 d3 EGF
5637 d2 C
5637 d2 EGF
5637 d3 C
5637 d3 EGF
Erk1/2
pAKT
B-act
pAKT
200
150
100
50
0
T24 Control
T24 EGF
5637 Control
5637 EGF
ERK1_2
200
150
100
50
0
T24 Control
T24 EGF
5637 Control
5637 EGF

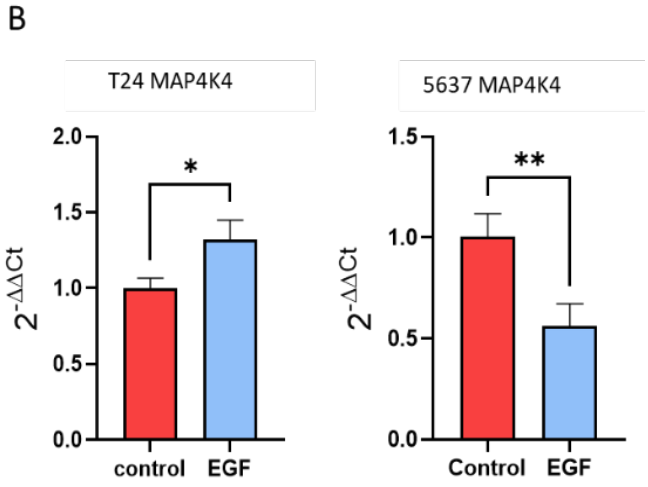

B
T24 MAP4K4
2.0
1.5
1.0
0.5
0.0
*
2-ΔΔCt
control
EGF
5637 MAP4K4
1.5
1.0
0.5
0.0
**
2-ΔΔCt
Control
EGF

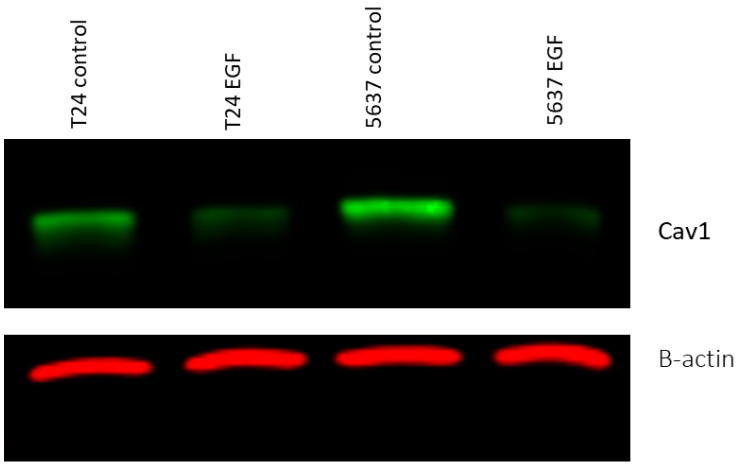
Figure 18 Akt/Erk pathway activation analysis A) Western blot images (Upper panel) and quantitative analysis of Western blot results (Lower panel). ß-actin protein was used as internal control B) Bar plots show the expression level of MAP4K4 gene.

*(Welch's t test p value = T24: 0,0390 5637: 0,0087) (*p < 0.05; **p < 0.01; ***p < 0.001)*

4.1.9. EGF treatment downregulates CAV1.

It has been known that EGF signaling induces the caveolin- dependent internalization of E-cadherin. *CAV1* has a role in cell-to-cell interaction and E-cadherin/ β-catenin complex disruption and β-catenin localization (Lu et al., 2003) It also causes the release of β-catenin and drives its accumulation to nucleus. Also, findings reveal that EGF signaling suppress the *CAV1* expression and *CAV1* downregulation indirectly suppresses the E-cadherin expression. (Galbiati et al., 2000)

To confirm the findings of literature and qRT- PCR data in Figure 20, Cav1 expression in protein level was analyzed with Western Blot. It was identified that Cav1 expression was significantly decreased at protein level after EGF treatment in both T24 and 5637 cell lines. Results shows that EGF treatment has a negative effect on Caveolin 1 expression.



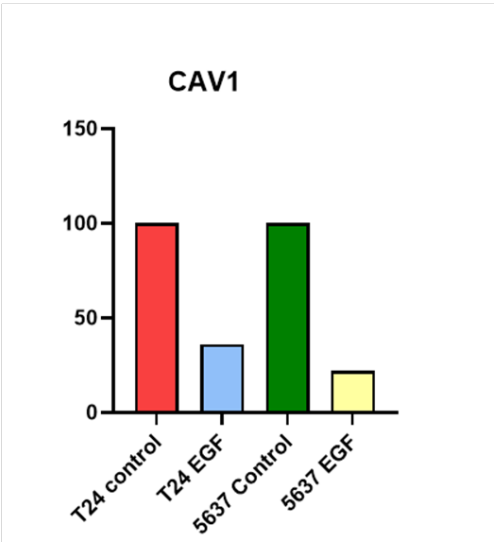


Figure 19 Western blot images of CAV1 (Left panel) and the bants were quantified by normalization with control values (Right panel). ß-actin protein was used as internal control.

4.1.10. EGF treatment increases nuclear localization of β-catenin.

It has been known that there is an association between β-catenin accumulation and disruption of caveola and E-cadherin formation. When the E-cadherin-caveolin and βcatenin complex are disrupted, β-catenin is releasing cytoplasm and eventually translocate to the nucleus (Galbiati et al., 2000; Lu et al., 2003). To be able to observe and analyze the β-catenin nuclear accumulation, EGF treated, and control cells were stained with β-catenin antibody and nuclear area intensity was measured. With the IF staining it was confirmed that nuclear accumulation of β-catenin increases with EGF treatment.

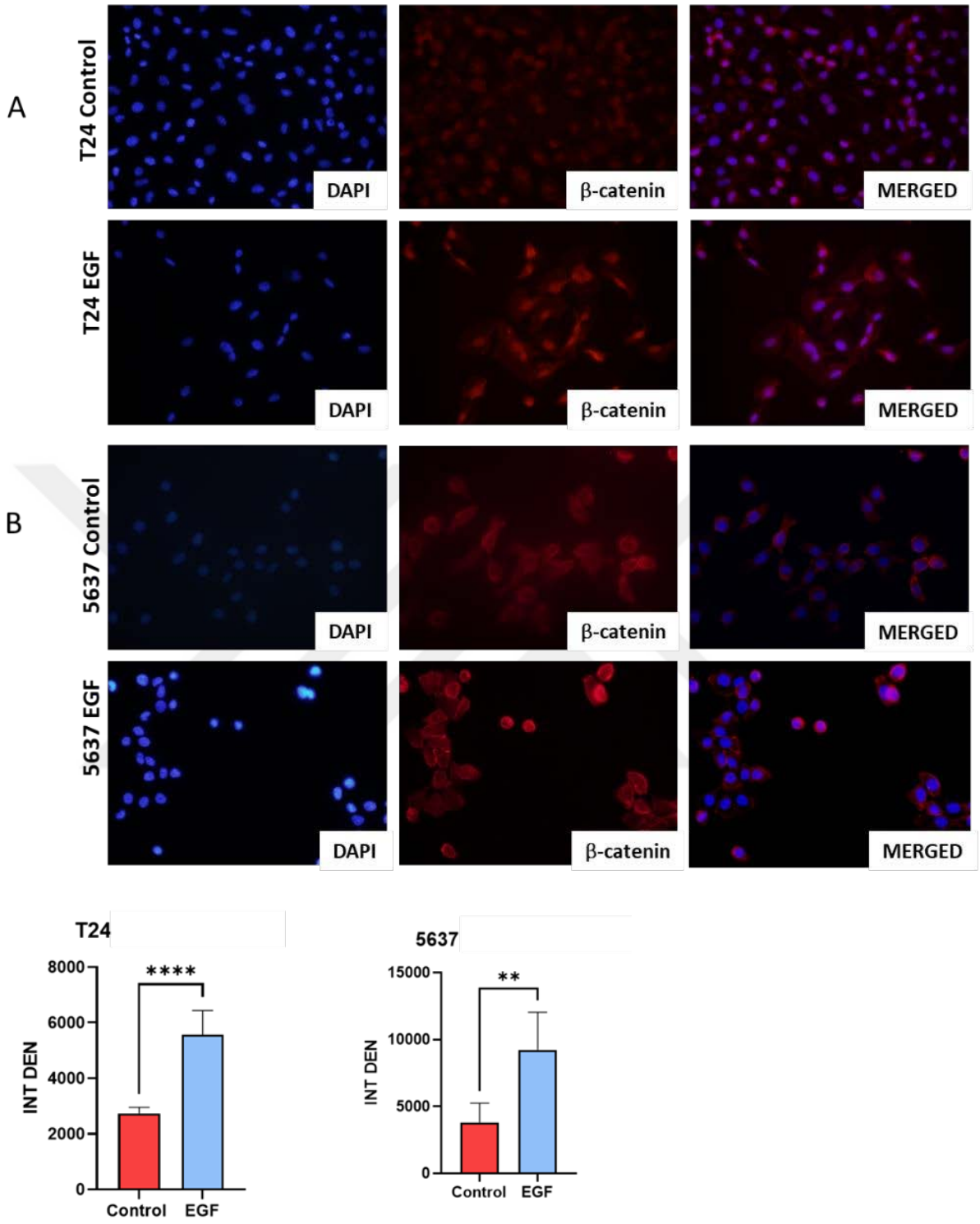
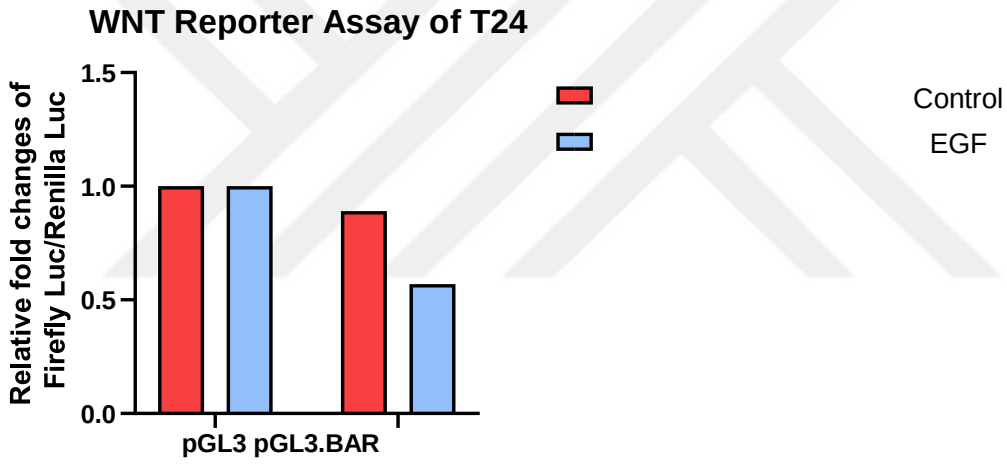


*Figure 20 Immunofluorescence staining showing the nuclear localization β-catenin (Upper panel) in T24 (A) and 5637 (B). (Lower panel) Intensity density analysis of the images (Welch's t test p value = T24: <0.0001 5637: 0,0087) (*p < 0.05; **p < 0.01; ***p < 0.001) (Experiment performed with at least 6 technical replicates)*

4.1.11. EGF induce the WNT signaling pathway.

To analyze the changes in WNT signaling, WNT reporter assay was performed in both T24 and 5637 cell lines comparing EGF treated and control cell lines (Figure 15). After 24 hours of EGF treatment, TCF7/LEF1 expression was measured by luciferase reporter assay. In 5637 cell line, as expected, TCF7/LEF1 expression was increased, and it can be said that WNT signaling pathway was induced. However, there was a decrease in TCF7/LEF1 expression in T24 cell line, which was unexpected as there was an increase in nuclear localization of β-catenin in T24 cell line as well. Therefore, this result requires additional analysis and experiments. Although there were some differences between 2 cell lines, results showed that EGF treatment likely induce WNT signaling pathway and TCF7/LEF1 transcriptional activity was increased.



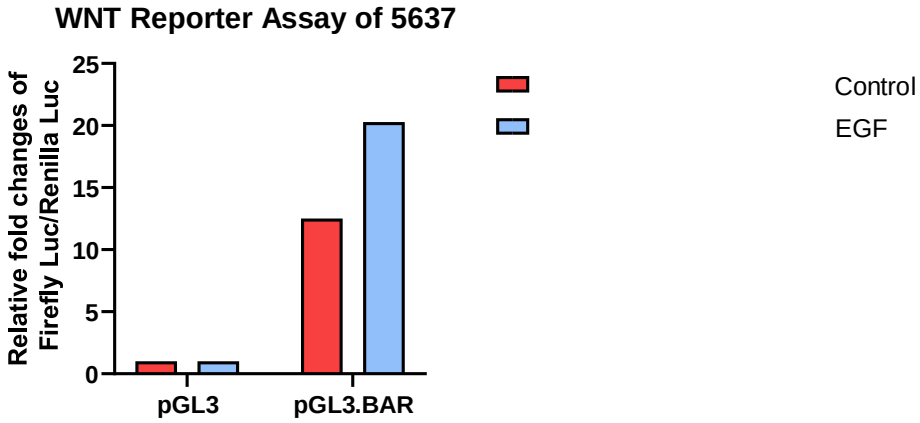


Figure 21 WNT reporter assay analysis of T24 and 5637 cell lines normalizing to basic pGL3- basic control plasmid. (Experiment performed with 3 technical replicates)

4.2. Gene Editing/ Gene-Character Change Based Neuroendocrine Modeling

Based on our previous study, it was identified that active chromatin regions specific to neuronal (neuroendocrine -like) molecular subtype of bladder cancer is involved in the expression of genes involved in WNT signaling and are enriched for TCF7/LEF1 transcription motifs. Additionally, it was identified that mutations in *CTNNB1* gene was much more frequent in neuronal subtype compared to other subtypes (Eray et al.,
2020). This result indicates that WNT/β-catenin signaling has role in regulation of NElike Bladder cancer. Further, performing an analysis to identify the genes most frequently mutated together with *CTNNB1* in the neuronal subtype, it was determined that *ARID1A* and *KRAS* were the most commonly mutated genes in addition to *CTNNB1*.



Figure 22 Mutation analysis in neuroendocrine-like bladder cancer. Oncoprint image shows the genes most frequently mutated together (KLF5, TSC22D1,KRAS, ARID1A) or mutually exclusive (TP53) with CTNNB1 in urothelium carcinoma samples belonging to the neuroendocrine-like molecular group. Image was created using cbioportal.

Therefore, establishment of neuroendocrine differentiated bladder cancer cell line models were aimed using different combinations of mutated CTNNB1, ARID1A and KRAS genes. Selected mutations which will be used are shown in Figure 23.

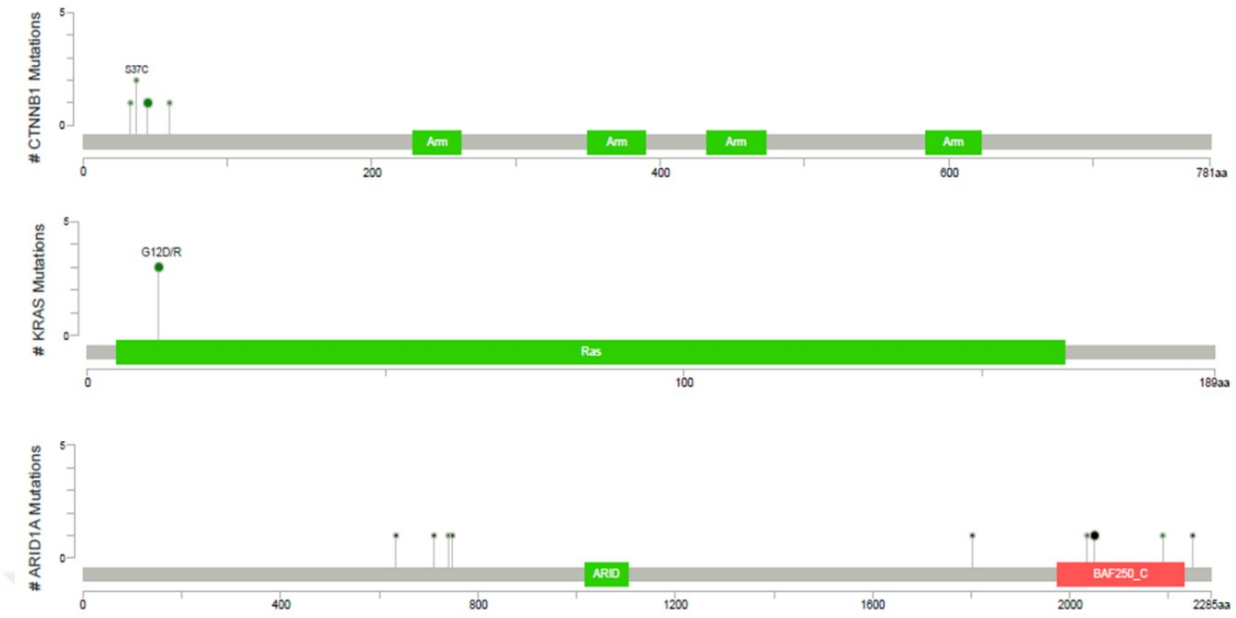


Figure 23 Mutations in CTNNB1, KRAS and ARID1A genes in neuroendocrine-like bladder cancers. The S45F point mutation in the CTNNB1 gene is indicated by the large green circle, the G12D point mutation in the KRAS gene is indicated by the large green circle and the W2050 point mutation in the ARID1A gene is indicated by the large black circle.*

4.2.1. Establishment of Mutations by CRISPR/Cas9 HDR

4.2.2. In Vitro Cleavage assay shows that Cas9 and sgRNA works properly.

To analyze whether Cas9 and designed sgRNA work properly, In Vitro Cleavage assay was performed. For each sgRNA and DNA template, reaction was performed and analyzed with agarose gel. It was identified that each sgRNA-Cas9 component successfully cleaved the DNA template (Figure 24). While the cleavage efficiency was low, incubation time optimization was performed with CTNNB1 sgRNA (Figure 25). These experiments are ongoing, once the steps ‘preparation of ribonucleo protein (RNP) complex with a molar ratio 1:1.2 Cas9: gRNA and nucleofection to the SV-HUC1 cell line with Homology Directed Repair (HDR) template’ are also done, mutant gene will be generated in SV-HUC 1 cell line.

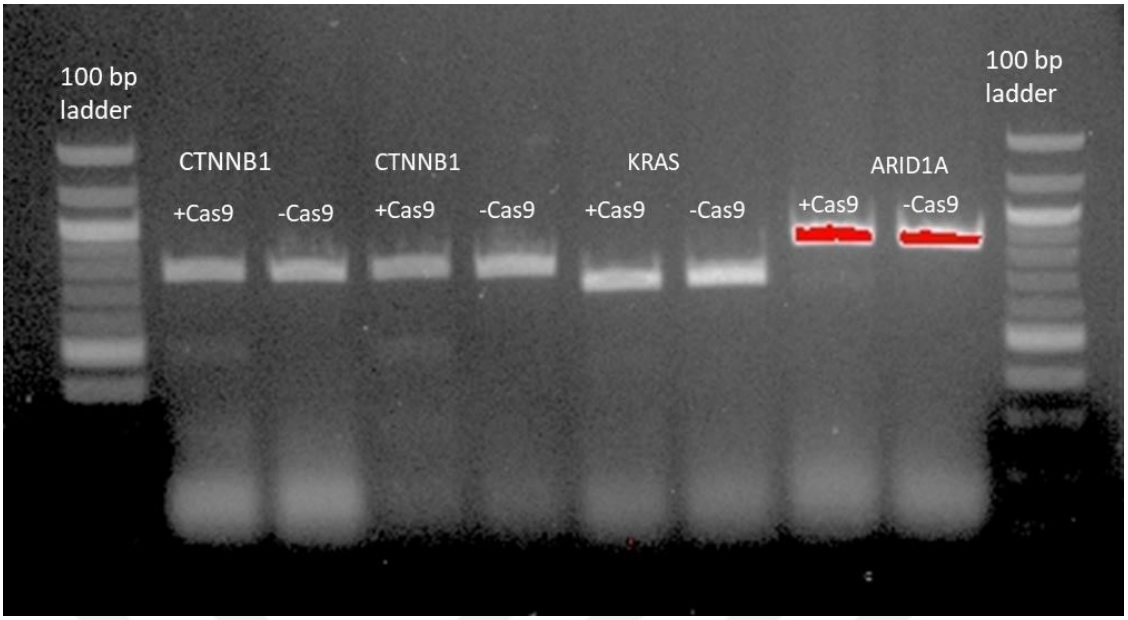


Figure 24 In vitro cleavage assay gel images. For CTNNB1, 2 different CTNNB1 sgRNA-Cas9 components was used to cleavage template DNA although sgRNA sequences was same. Incubation of cleavage was 30 second.

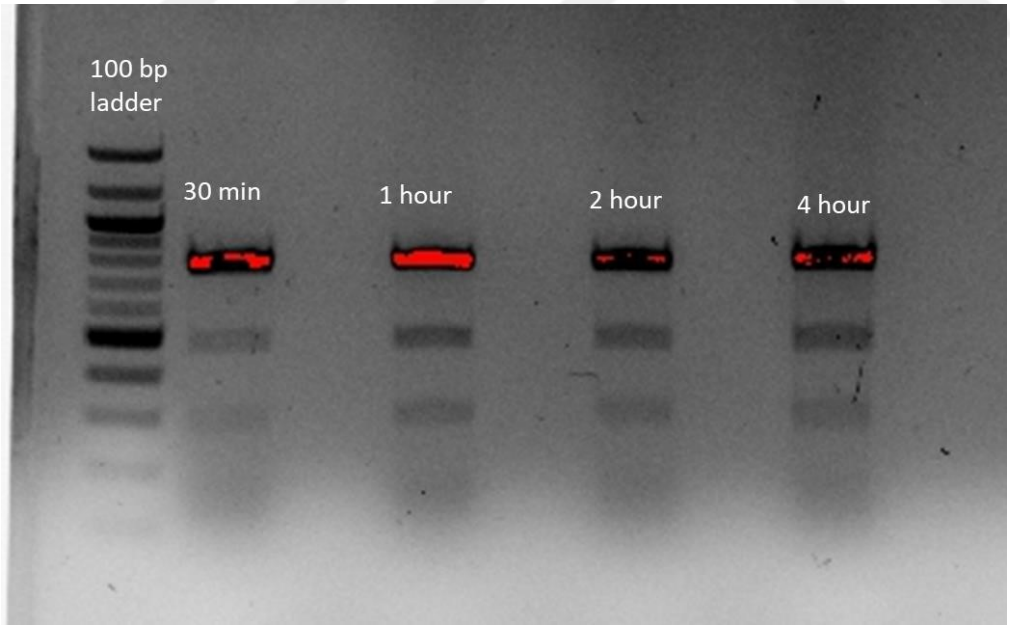


Figure 25 In vitro cleavage incubation time optimization. CTNNB1 sgRNA-Cas9 complex was used for In vitro cleavage assay. 30 minutes, 1 hour, 2 hour and 4 hour incubation results were analyzed.

4.2.3. Overexpression of Mutant Genes

4.2.3.1. PHAGE-KRAS-G12D plasmid was transduced to SV-HUC-1 cell line using lentiviral transduction.

OnceSV-HUC-1 cell line was transduced with PHAGE-KRAS-G12D plasmid, cells were sorted both as single and bulk (Figure 26). These experiments are ongoing, protein isolation from bulk cells and mutation analysis from single cell colonies will be performed after the cells reach the required confluency.

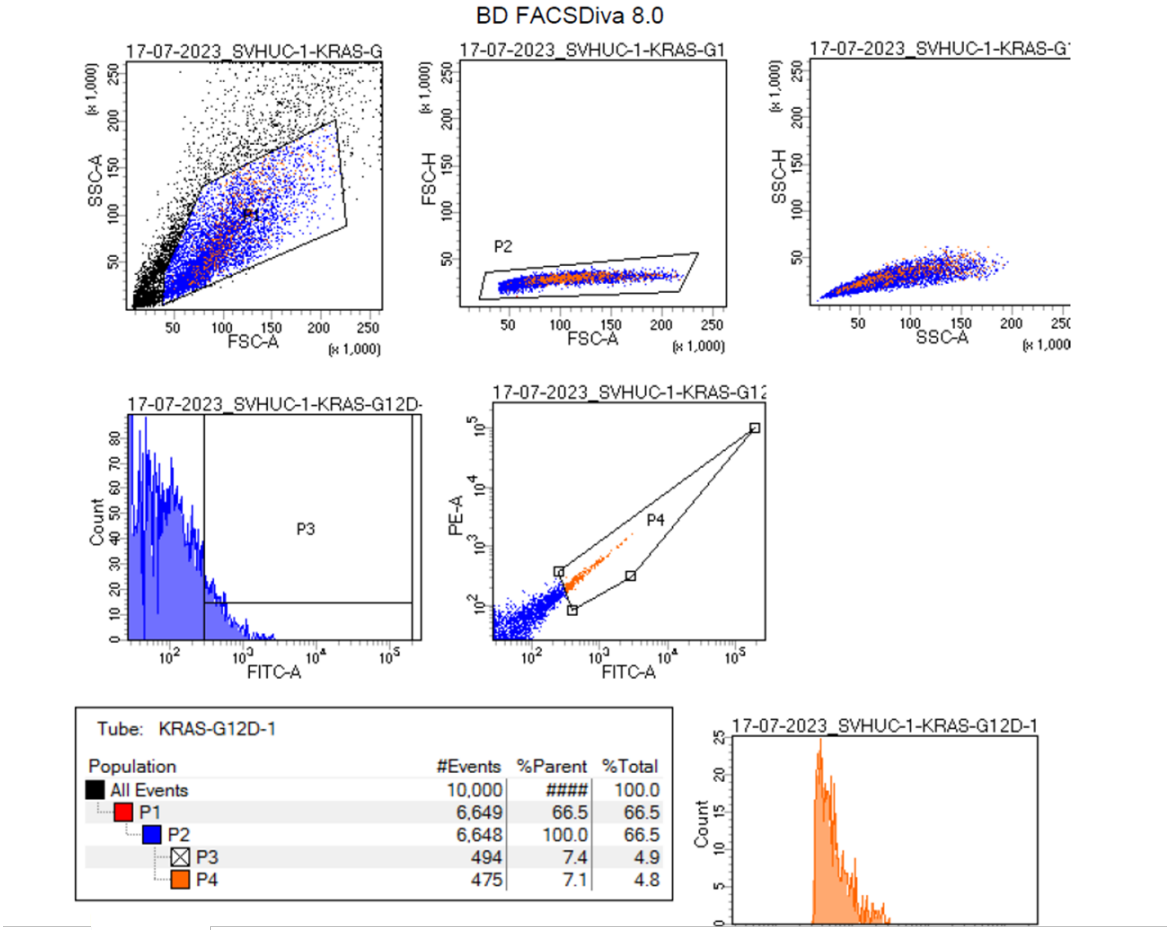


Figure 26 Flow cytometry analysis of PHAGE-KRAS-G12D transduced SV-HUC-1 cell line. Graphs show the GFP positive SV-HUC-1 cells which have the PHAGE-KRASG12D plasmid. According to GFP positivity, cells were sorted both as single and bulk.

5. DISCUSSION

There have been many studies for modeling neuroendocrine differentiation in many different cancer types such as prostate, colorectal or lung cancer using many different methods (Danza et al., 2012; Delk & Farach-Carson, 2012; Deng et al., 2008). However, there is almost no study about modeling of neuroendocrine differentiation in bladder cancer. Generation of neuroendocrine differentiation models is very important to understand the mechanisms of the differentiation, origin of the differentiated cells and response to the new treatment or combination of the treatments, and development of preclinical models for neuroendocrine and neuroendocrine-like bladder cancer, which shows the worst prognosis (Lissa et al., 2022; Puca et al., 2019).

In this study, we aimed to generate neuroendocrine differentiated bladder cells and understand the mechanism underlying differentiation and how the cellular processes were affected. There are several approaches and method to generate neuroendocrine differentiation. In this study, we planned to use two different approaches. In one approach, we induced bladder cancer cells with EGF, and trans differentiate them to neuroendocrine cells. After the trans differentiation, we analyzed the proliferation, cell to cell interaction and EMT characteristics. There have been many studies which explain how EGF affects the molecular signaling pathways and cause differentiation. EGF treatment causes E-cadherin downregulation and induces caveolin-dependent endocytosis of E-cadherin. These regulations cause disruption of cell-to-cell interaction, epithelial to mesenchymal transition (EMT) and neuroendocrine differentiation. Caveolin 1, which act as a tumor suppressor, also has connections with cell-to-cell interaction disruption and EMT. E-cadherin binds to β-catenin in cell membrane mediated with Cav-1. EGF treatment releases this complex, and β-catenin locates to the cytoplasm independently GSK3β. β-catenin eventually locates to the nucleus and accumulates there. Elevated β-catenin level in nucleus activates the βcatenin-TCF/LEF1 associated gene expression (Croager E, 2004; Galbiati et al., 2000; Lu et al., 2003). In this study, we showed downregulation of the E- cadherin and Cav1 expression both at mRNA and protein level after the EGF treatment and how these downregulations cause the EMT and neuroendocrine differentiation. Also, we managed to confirm nuclear localization of β-catenin after the EGF treatment. We could

additionally show the activation of WNT signaling pathway although there were some discrepancies in the analyzed cell lines. Further this study shows that after EGF treatment and neuroendocrine differentiation, cell to cell interaction decreases as it has been shown in literature (Lu et al., 2003).

In the second approach for modeling neuroendocrine differentiation, we aimed to follow gene editing/ gene-character change based method while introducing mutations in the genes which are likely critical for neuroendocrine differentiation which are CTNNB1-S45F, ARID1A W2050* and KRAS G12D mutations. We applied CRISPR/Cas9- HDR method, which is widely used in previous studies, (Modzelewski et al., 2018) to generate the mutations. However, because of the efficiency problem, we could not manage to make mutations yet. On the other hand, we could successfully show that our sgRNAs are able to target the genome at the mutation points we aimed and cleave with Cas9 protein (Figure 19). Here, we plan to enhance our protocol and increase the efficiency. Also, we tried to overexpress mutated version of our genes. At this point, we ordered the plasmids, primers, and enzymes. We also successfully transduced KRAS-G12D mutated version (Figure 20) and optimized the protocol. Overall, the second approach is still ongoing given the technical complexity of the used methods and lack of full expertise for the application of the methods. Once the mutant genes are successfully created and/or overexpressed, we will analyze the neuroendocrine differentiation, proliferation, determine chromatin organization and drug resistance.

This research and study are one of the first studies for modeling neuroendocrine differentiation in bladder cancer and the results have implications for diagnosis and treatment of neuroendocrine-like bladder cancer.

6. CONCLUSION AND FUTURE ASPECTS

In this thesis, we aimed to establish neuroendocrine-like bladder cancer cell lines and analyze the molecular and phenotypic affects. It has been known that specific mutations or specific inductions cause trans differentiation into neuroendocrine types. Mutational data analysis show that CTNNB1 is frequently mutated in

neuroendocrinelike bladder cancer tumors. KRAS and ARID1A mutations are also found in these tumors. Therefore, generation of these mutations is likely a way of obtaining neuroendocrine-like bladder cancer cell lines. We will analyze how these mutations affect the cells and whether cause neuroendocrine differentiation or not.

Also, some factors induce the lineage plasticity and trans differentiate epithelial cells to neuroendocrine-like cells. That's why we treated the cells with EGF and observed the neuronal characteristics. Further analysis will be beneficial to understand mechanism of neuroendocrine differentiation.

7. REFRENCES

Ahmad, I., Morton, J. P., Singh, L. B., Radulescu, S. M., Ridgway, R. A., Patel, S., Woodgett, J., Winton, D. J., Taketo, M. M., Wu, X. R., Leung, H. Y., & Sansom, O. J. (2011). B-Catenin activation synergizes with PTEN loss to cause bladder cancer formation. *Oncogene*, *30*(2), 178–189. https://doi.org/10.1038/onc.2010.399

Al-Ahmadie, H., & Netto, G. J. (2019). *Updates on the Genomics of Bladder Cancer and Novel Molecular Taxonomy*. http://links.lww.com/PAP/

Bellmunt, J., Hussain, M., & Dinney, C. P. (2003). Novel approaches with targeted therapies in bladder cancer: Therapy of bladder cancer by blockade of the epidermal growth factor receptor family. *Critical Reviews in Oncology/Hematology*, *46*(SUPPL.), 85–104. https://doi.org/10.1016/S10408428(03)00067-2

Bian, J., Dannappel, M., Wan, C., & Firestein, R. (2020). Transcriptional Regulation of Wnt/β-Catenin Pathway in Colorectal Cancer. In *Cells* (Vol. 9, Issue 9). NLM (Medline). https://doi.org/10.3390/cells9092125

Black, A. J., & Black, P. C. (2020). Variant histology in bladder cancer: Diagnostic and clinical implications. *Translational Cancer Research*, *9*(10), 6565–6575. https://doi.org/10.21037/tcr-20-2169

Bugter, J. M., Fenderico, N., & Maurice, M. M. (2021). Mutations and mechanisms of

WNT pathway tumour suppressors in cancer. In *Nature Reviews Cancer* (Vol. 21, Issue 1, pp. 5–21). Nature Research. https://doi.org/10.1038/s41568-020-00307z

Chandrasekar, T., Erlich, A., & Zlotta, A. R. (2018). Molecular Characterization of Bladder Cancer. In *Current Urology Reports* (Vol. 19, Issue 12). Current Medicine Group LLC 1. https://doi.org/10.1007/s11934-018-0853-5

Chang, K.-T., Huang, C.-Y. F., Tsai, C.-M., Chiu, C.-H., & Lok, Y.-Y. (2005). Role of IL-6 in neuroendocrine differentiation and chemosensitivity ofnon-small cell lung cancer. *Am J Physiol Lung Cell Mol Physiol*, *289*, 438–445. https://doi.org/10.1152/ajplung.00033.2005.-Interleu

Chang, Y., Kim, S. Y., Choi, Y. J., So, K. S., Rho, J. K., Kim, W. S., Lee, J. C., Chung, J. H., & Choi, C. M. (2013). Neuroendocrine differentiation in acquired resistance to epidermal growth factor receptor tyrosine kinase inhibitor. *Tuberculosis and Respiratory Diseases*, *75*(3), 95–103. https://doi.org/10.4046/trd.2013.75.3.95

Cortés, M. A., Cariaga-Martinez, A. E., Lobo, M. V. T., Martín orozco, R. M., Motiño, O., Rodríguez-Ubreva, F. J., Angulo, J., López-Ruiz, P., & Colás, B. (2012). EGF promotes neuroendocrine-like differentiation of prostate cancer cells in the presence of LY294002 through increased ErbB2 expression independent of the phosphatidylinositol 3-kinase-AKT pathway. *Carcinogenesis*, *33*(6), 1169–1177. https://doi.org/10.1093/carcin/bgs139

Da Costa, J. B., Gibb, E. A., Bivalacqua, T. J., Liu, Y., Zarni Oo, H., Miyamoto, D. T., Alshalalfa, M., Davicioni, E., Wright, J., Dall'Era, M. A., Douglas, J., Boormans, J. L., Van Der Heijden, M. S., Wu, C. L., Van Rhijn, B. W. G., Gupta, S., Grivas, P., Mouw, K. W., Murugan, P., … Black, P. C. (2019). Molecular characterization of neuroendocrinelike bladder cancer. *Clinical Cancer Research*, *25*(13), 3908–3920. https://doi.org/10.1158/1078-0432.CCR-18-3558

Danza, G., Di Serio, C., Rosati, F., Lonetto, G., Sturli, N., Kacer, D., Pennella, A., Ventimiglia, G., Barucci, R., Piscazzi, A., Prudovsky, I., Landriscina, M., Marchionni, N., & Tarantini, F. (2012). Notch signaling modulates hypoxia-induced

neuroendocrine differentiation of human prostate cancer cells. *Molecular Cancer Research*, *10*(2), 230–238. https://doi.org/10.1158/1541-7786.MCR-11-0296

Delk, N. A., & Farach-Carson, M. C. (2012). Interleukin-6: A bone marrow stromal cell paracrine signal that induces neuroendocrine differentiation and modulates autophagy in bone metastatic PCa cells. *Autophagy*, *8*(4), 650–663. https://doi.org/10.4161/auto.19226

Deng, X., Liu, H., Huang, J., Cheng, L., Keller, E. T., Parsons, S. J., & Hu, C. D. (2008). Ionizing radiation induces prostate cancer neuroendocrine differentiation through interplay of CREB and ATF2: Implications for disease progression. *Cancer Research*, *68*(23), 9663–9670. https://doi.org/10.1158/0008-5472.CAN-08-2229

Dong, B., Miao, J., Wang, Y., Luo, W., Ji, Z., Lai, H., Zhang, M., Cheng, X., Wang, J., Fang, Y., Zhu, H. H., Chua, C. W., Fan, L., Zhu, Y., Pan, J., Wang, J., Xue, W., & Gao, W. Q. (2020). Single-cell analysis supports a luminal-neuroendocrine transdifferentiation in human prostate cancer. *Communications Biology*, *3*(1). https://doi.org/10.1038/s42003-020-01476-1

Eray, A., & Erkek-özhan, S. (2021). Classification of bladder cancer cell lines according to regulon activity. *Turkish Journal of Biology*, *45*(6), 656–666. https://doi.org/10.3906/biy-2107-72

Eray, A., Güneri, P. Y., Yılmaz, G. Ö., Karakülah, G., & Erkek-Ozhan, S. (2020). Analysis of open chromatin regions in bladder cancer links β-catenin mutations and Wnt signaling with neuronal subtype of bladder cancer. *Scientific Reports*, *10*(1). https://doi.org/10.1038/s41598-020-75688-0

Fong, M. H. Y., Feng, M., McConkey, D. J., & Choi, W. (2020). Update on bladder cancer molecular subtypes. *Translational Andrology and Urology*, *9*(6), 2881–2889. https://doi.org/10.21037/tau-2019-mibc-12

Galbiati, F., Volonte, D., Brown, A. M. C., Weinstein, D. E., Ben-Ze'ev, A., Pestell, R. G., & Lisantia, M. P. (2000). Caveolin-1 expression inhibits Wnt/β-catenin/Lef-1 signaling by recruting β-catenin to caveolae membrane domains. *Journal of*

Biological Chemistry, *275*(30), 23368–23377. https://doi.org/10.1074/jbc.M002020200

Gao, X., Chen, G., Gao, C., Zhang, D. H., Kuan, S. F., Stabile, L. P., Liu, G., & Hu, J. (2017). MAP4K4 is a novel MAPK/ERK pathway regulator required for lung adenocarcinoma maintenance. *Molecular Oncology*, *11*(6), 628–639. https://doi.org/10.1002/1878-0261.12055

Garg, M., & Maurya, N. (2019). WNT/β-catenin signaling in urothelial carcinoma of bladder. *World J Nephrol*, *8*(5), 83–94. https://doi.org/10.5527/wjn.v8.i5.83

Grivas, P., Bismar, T. A., Alva, A. S., Huang, H. C., Liu, Y., Seiler, R., Alimohamed, N., Cheng, L., Hyndman, M. E., Dabbas, B., Black, P. C., Davicioni, E., Wright, J. L., Ornstein, M. C., Mian, O. Y., Kaimakliotis, H. Z., Gibb, E. A., & Lotan, Y. (2020). Validation of a neuroendocrine-like classifier confirms poor outcomes in patients with bladder cancer treated with cisplatin-based neoadjuvant chemotherapy. *Urologic Oncology: Seminars and Original Investigations*, *38*(4), 262–268. https://doi.org/10.1016/j.urolonc.2019.11.004

Grossmann, T. N., Yeh, J. T. H., Bowman, B. R., Chu, Q., Moellering, R. E., & Verdine, G. L. (2012). Inhibition of oncogenic Wnt signaling through direct targeting of βcatenin. *Proceedings of the National Academy of Sciences of the United States of America*, *109*(44), 17942–17947. https://doi.org/10.1073/pnas.1208396109

Heuberger, J., & Birchmeier, W. (2010). Interplay of cadherin-mediated cell adhesion and canonical Wnt signaling. In *Cold Spring Harbor perspectives in biology* (Vol. 2, Issue 2). https://doi.org/10.1101/cshperspect.a002915

Huang, Z., Zhang, M., Chen, G., Wang, W., Zhang, P., Yue, Y., Guan, Z., Wang, X., & Fan, J. (2019). Bladder cancer cells interact with vascular endothelial cells triggering EGFR signals to promote tumor progression. *International Journal of Oncology*, *54*(5), 1555–1566. https://doi.org/10.3892/ijo.2019.4729

Iacovino, M. L., Miceli, C. C., De Felice, M., Barone, B., Pompella, L., Chiancone, F., Di Zazzo, E., Tirino, G., Della Corte, C. M., Imbimbo, C., De Vita, F., & Crocetto, F. (2022). Novel Therapeutic Opportunities in Neoadjuvant Setting in Urothelial

Cancers: A New Horizon Opened by Molecular Classification and Immune Checkpoint Inhibitors. In *International Journal of Molecular Sciences* (Vol. 23, Issue 3). MDPI. https://doi.org/10.3390/ijms23031133

Jalanko, T., de Jong, J. J., Gibb, E. A., Seiler, R., & Black, P. C. (2020). Genomic Subtyping in Bladder Cancer. In *Current Urology Reports* (Vol. 21, Issue 2). Springer. https://doi.org/10.1007/s11934-020-0960-y

Kamoun, A., de Reyniès, A., Allory, Y., Sjödahl, G., Robertson, A. G., Seiler, R., Hoadley, K. A., Groeneveld, C. S., Al-Ahmadie, H., Choi, W., Castro, M. A. A., Fontugne, J., Eriksson, P., Mo, Q., Kardos, J., Zlotta, A., Hartmann, A., Dinney, C. P., Bellmunt, J., … Weinstein, J. (2020). A Consensus Molecular Classification of Muscle-invasive Bladder Cancer[Formula presented]. *European Urology*, *77*(4), 420–433. https://doi.org/10.1016/j.eururo.2019.09.006

Kim, J. T., Li, J., Jang, E. R., Gulhati, P., Rychahou, P. G., Napier, D. L., Wang, C., Weiss, H. L., Lee, E. Y., Anthony, L., Townsend, C. M., Liu, C., & Evers, B. M. (2013). Deregulation of Wnt/β-catenin signaling through genetic or epigenetic alterations in human neuroendocrine tumors. *Carcinogenesis*, *34*(5), 953–961. https://doi.org/10.1093/carcin/bgt018

Lenis, A. T., Lec, P. M., & Chamie, K. (2020). Bladder cancer a review. In *JAMA - Journal of the American Medical Association* (Vol. 324, Issue 19, pp. 1980–1991). American Medical Association. https://doi.org/10.1001/jama.2020.17598

Lin, T.-P., Chang, Y.-T., Lee, S.-Y., Campbell, M., Wang, T.-C., Shen, S.-H., Chung, H.-J., Chang, Y.-H., Chiu, A. W., Pan, C.-C., Lin, C.-H., Chu, C.-Y., Kung, H.-J., Cheng, C.-Y., & Chang, P.-C. (2016). REST reduction is essential for hypoxiainduced neuroendocrine differentiation of prostate cancer cells by activating autophagy signaling. In *Oncotarget* (Vol. 7, Issue 18). www.impactjournals.com/oncotarget/

Lindskrog, S. V., Prip, F., Lamy, P., Taber, A., Groeneveld, C. S., Birkenkamp-Demtröder, K., Jensen, J. B., Strandgaard, T., Nordentoft, I., Christensen, E., Sokac, M., Birkbak, N. J., Maretty, L., Hermann, G. G., Petersen, A. C., Weyerer,

V., Grimm, M. O., Horstmann, M., Sjödahl, G., … Dyrskjøt, L. (2021). An integrated multi-omics analysis identifies prognostic molecular subtypes of non-muscleinvasive bladder cancer. *Nature Communications*, *12*(1). https://doi.org/10.1038/s41467-021-22465-w

Lissa, D., Takahashi, N., Desai, P., Manukyan, I., Schultz, C. W., Rajapakse, V., Velez, M. J., Mulford, D., Roper, N., Nichols, S., Vilimas, R., Sciuto, L., Chen, Y., Guha, U., Rajan, A., Atkinson, D., El Meskini, R., Weaver Ohler, Z., & Thomas, A. (2022). Heterogeneity of neuroendocrine transcriptional states in metastatic small cell lung cancers and patient-derived models. *Nature Communications*, *13*(1). https://doi.org/10.1038/s41467-022-29517-9

Liu, Y., Patel, L., Mills, G. B., Lu, K. H., Sood, A. K., Ding, L., Kucherlapati, R., Mardis, E. R., Levine, D. A., Shmulevich, I., Broaddus, R. R., & Zhang, W. (2014). Clinical significance of CTNNB1 mutation and Wnt pathway activation in endometrioid endometrial carcinoma. *Journal of the National Cancer Institute*, *106*(9). https://doi.org/10.1093/jnci/dju245

Lu, Z., Ghosh, S., Wang, Z., & Hunter, T. (2003). *Downregulation of caveolin-1 function by EGF leads to the loss of E-cadherin, increased transcriptional activity ofcatenin, and enhanced tumor cell invasion*.

Masuda, H., Zhang, D., Bartholomeusz, C., Doihara, H., Hortobagyi, G. N., & Ueno, N. T. (2012). Role of epidermal growth factor receptor in breast cancer. In *Breast Cancer Research and Treatment* (Vol. 136, Issue 2, pp. 331–345). https://doi.org/10.1007/s10549-012-2289-9

McConkey, D. J., & Choi, W. (2018). Molecular Subtypes of Bladder Cancer. In *Current Oncology Reports* (Vol. 20, Issue 10). Current Medicine Group LLC 1. https://doi.org/10.1007/s11912-018-0727-5

Mooso, B. A., Vinall, R. L., Mudryj, M., Yap, S. A., deVere White, R. W., & Ghosh, P. M. (2015). The Role of EGFR Family Inhibitors in Muscle Invasive Bladder Cancer: A Review of Clinical Data and Molecular Evidence. In *Journal of Urology* (Vol. 193, Issue 1, pp. 19–29). Elsevier Inc. https://doi.org/10.1016/j.juro.2014.07.121

Moschini, M., D'Andrea, D., Korn, S., Irmak, Y., Soria, F., Compérat, E., & Shariat, S. F. (2017). Characteristics and clinical significance of histological variants of bladder cancer. In *Nature Reviews Urology* (Vol. 14, Issue 11, pp. 651–668). Nature Publishing Group. https://doi.org/10.1038/nrurol.2017.125

Mrozik, K. M., Blaschuk, O. W., Cheong, C. M., Zannettino, A. C. W., & Vandyke, K. (2018). N-cadherin in cancer metastasis, its emerging role in haematological malignancies and potential as a therapeutic target in cancer. In *BMC Cancer* (Vol. 18, Issue 1). BioMed Central Ltd. https://doi.org/10.1186/s12885-018-4845-0

Park, J. W., Lee, J. K., Sheu, K. M., Wang, L., Balanis, N. G., Nguyen, K., Smith, B. A., Cheng, C., Tsai, B. L., Cheng, D., Huang, J., Kurdistani, S. K., Graeber, T. G., & Witte, O. N. (2018). *Reprogramming normal human epithelial tissues to a common, lethal neuroendocrine cancer lineage*. http://science.sciencemag.org/

Plissonnier, M. L., Fauconnet, S., Bittard, H., & Lascombe, I. (2011). The antidiabetic drug ciglitazone induces high grade bladder cancer cells apoptosis through the up-regulation of trail. *PLoS ONE*, *6*(12). https://doi.org/10.1371/journal.pone.0028354

Puca, L., Vlachostergios, P. J., & Beltran, H. (2019). Neuroendocrine differentiation in prostate cancer: Emerging biology, models, and therapies. *Cold Spring Harbor Perspectives in Medicine*, *9*(2). https://doi.org/10.1101/cshperspect.a030593

Ringuette-Goulet, C., Bolduc, S., & Pouliot, F. (2018). Modeling human bladder cancer. *World Journal of Urology*, *36*(11), 1759–1766. https://doi.org/10.1007/s00345018-2369-5

Robertson, A. G., Kim, J., Al-Ahmadie, H., Bellmunt, J., Guo, G., Cherniack, A. D., Hinoue, T., Laird, P. W., Hoadley, K. A., Akbani, R., Castro, M. A. A., Gibb, E. A., Kanchi, R. S., Gordenin, D. A., Shukla, S. A., Sanchez-Vega, F., Hansel, D. E., Czerniak, B. A., Reuter, V. E., … Zwarthoff, E. C. (2017). Comprehensive Molecular Characterization of Muscle-Invasive Bladder Cancer. *Cell*, *171*(3), 540-556.e25. https://doi.org/10.1016/j.cell.2017.09.007

Sanli, O., Dobruch, J., Knowles, M. A., Burger, M., Alemozaffar, M., Nielsen, M. E., & Lotan, Y. (2017). Bladder cancer. *Nature Reviews Disease Primers*, *3*. https://doi.org/10.1038/nrdp.2017.22

Sasaki, T., Hiroki, K., & Yamashita, Y. (2013). The role of epidermal growth factor receptor in cancer metastasis and microenvironment. In *BioMed Research International* (Vol. 2013). https://doi.org/10.1155/2013/546318

Shen, P., Jing, Y., Zhang, R., Cai, M. C., Ma, P., Chen, H., & Zhuang, G. (2018). Comprehensive genomic profiling of neuroendocrine bladder cancer pinpoints molecular origin and potential therapeutics. *Oncogene*, *37*(22), 3039–3044. https://doi.org/10.1038/s41388-018-0192-5

Sijia Wang, Z. Z. H. P. , K. Z. (2019). Recent advances on the roles of epidermal growth factor receptor in psoriasis. *American Journal of Translational Research*, *11*(2), 520–528.

Soh, M., Dunlevy, J. R., Garrett, S. H., Allen, C., Sens, D. A., Zhou, X. D., Sens, M. A., & Somji, S. (2012). Increased neuron specific enolase expression by urothelial cells exposed to or malignantly transformed by exposure to Cd 2+ or As 3+. *Toxicology Letters*, *212*(1), 66–74. https://doi.org/10.1016/j.toxlet.2012.05.003

Spiotto, M. T., & Chung, T. D. K. (2000). STAT3 Mediates IL-6-Induced Neuroendocrine Differentiation in Prostate Cancer Cells. In *Prostate* (Vol. 42).

Sung, H., Ferlay, J., Siegel, R. L., Laversanne, M., Soerjomataram, I., Jemal, A., & Bray, F. (2021). Global Cancer Statistics 2020: GLOBOCAN Estimates of Incidence and Mortality Worldwide for 36 Cancers in 185 Countries. *CA: A Cancer Journal for Clinicians*, *71*(3), 209–249. https://doi.org/10.3322/caac.21660

Tan, T. Z., Rouanne, M., Tan, K. T., Huang, R. Y. J., & Thiery, J. P. (2019). Molecular Subtypes of Urothelial Bladder Cancer: Results from a Meta-cohort Analysis of 2411 Tumors. *European Urology*, *75*(3), 423–432. https://doi.org/10.1016/j.eururo.2018.08.027

Thomas, R., & Weihua, Z. (2019). Rethink of EGFR in cancer with its kinase independent function on board. *Frontiers in Oncology*, *9*(AUG). https://doi.org/10.3389/fonc.2019.00800

Uribe, M. L., Marrocco, I., & Yarden, Y. (2021). *cancers EGFR in Cancer: Signaling Mechanisms, Drugs, and Acquired Resistance*. https://doi.org/10.3390/cancers

Wang, L., Smith, B. A., Balanis, N. G., Tsai, B. L., Nguyen, K., Cheng, M. W., Obusan, M. B., Esedebe, N., Patel, S. J., Zhang, H., Clark, P. M., Sisk, A. E., Said, J. W., Huang, J., Graeber, T. G., Witte, O. N., Chin, A. I., Park, J. W., Hsieh, A. C., & Liao, J. C. (2020). *A genetically defined disease model reveals that urothelial cells can initiate divergent bladder cancer phenotypes*. https://doi.org/10.1073/pnas.1915770117/-/DCSupplemental

Wang, Y., Wang, Y., Ci, X., Choi, S. Y. C., Crea, F., Lin, D., & Wang, Y. (2021). Molecular events in neuroendocrine prostate cancer development. In *Nature Reviews Urology* (Vol. 18, Issue 10, pp. 581–596). Nature Research. https://doi.org/10.1038/s41585-021-00490-0

Wen, X., Wu, Y., Awadasseid, A., Tanaka, Y., & Zhang, W. (2020). New advances in canonical wnt/β-catenin signaling in cancer. In *Cancer Management and Research* (Vol. 12, pp. 6987–6998). Dove Medical Press Ltd. https://doi.org/10.2147/CMAR.S258645

Xia, K., Zhong, W., Chen, J., Lai, Y., Huang, G., Liu, H., Dong, W., He, W., Lin, T., & Huang, J. (2020). Clinical Characteristics, Treatment Strategy, and Outcomes of Primary Large Cell Neuroendocrine Carcinoma of the Bladder: A Case Report and Systematic Review of the Literature. *Frontiers in Oncology*, *10*. https://doi.org/10.3389/fonc.2020.01291

Xie, Y., Ning, S., & Hu, J. (2022). Molecular mechanisms of neuroendocrine differentiation in prostate cancer progression. In *Journal of Cancer Research and Clinical Oncology* (Vol. 148, Issue 7, pp. 1813–1823). Springer Science and Business Media Deutschland GmbH. https://doi.org/10.1007/s00432-022-040617

Yang, G., Bondaruk, J., Cogdell, D., Wang, Z., Lee, S., Lee, J. G., Zhang, S., Choi, W., Wang, Y., Liang, Y., Wang, G., Wang, Y., Yao, H., Dadhania, V., Gao, J., Logothetis, C., Siefker-Radtke, A., Kamat, A., Dinney, C., … Czerniak, B. (2020). Urothelial-to-Neural Plasticity Drives Progression to Small Cell Bladder Cancer. *IScience*, *23*(6). https://doi.org/10.1016/j.isci.2020.101201

Zhu, Y., Liu, C., Cui, Y., Nadiminty, N., Lou, W., & Gao, A. C. (2014). Interleukin-6 induces neuroendocrine differentiation (NED) through suppression of RE-1 silencing transcription factor (REST). *Prostate*, *74*(11), 1086–1094. https://doi.org/10.1002/pros.22819

8. APPENDİX

8.1. Research Ethics Committee Approval

İZMİR BİYOTIP VE GENOM MERKEZİ
GİRİŞİMSEL OLMAYAN ARAŞTIRMALAR ETİK KURULU (İBG-GOEK)
KARARI

Toplantı Tarihi	: 28/01/2022	**Toplantı Günü**	: Cuma
Toplantı Sayısı	: 1	**Toplantı Saati**	: 10:30

Sayın Doç. Dr. Şerif ŞENTÜRK,

2022-002 Protokol No'lu; sorumlusu olduğunuz "Mesane Kanserinde Nöroendokrin Farklılaşmanın Modellenmesi ve Fenotipik ve Moleküler Etkilerinin Araştırılması" başlıklı araştırmanın uygulanmasında etik açıdan sakınca olmadığına oy birliği ile karar verilmiştir.

Bilgilerinizi ve gereğini rica ederiz.

Dr. Serap ERKEK ÖZHAN
Başkan V.

Pandemi süresince online ortamda gerçekleştirilen toplantımızda alınan kararlar tek imzalı olarak düzenlenmektedir. Pandemi sona erdikten sonra ıslak imzalı karar belgesi teslim edilecektir.



EZGİ BOYVATLI

Personal Information

Contact Information

Contact Address	A 8/27.sok
Telephone	(5
Email	e
Web Page	

Education Information

01 August 2023 - Now (1 Month)
Doktora, Doktora, DOKUZ EYLÜL ÜNİVERSİTESİ, TÜRKİYE
İZMİR ULUSLARARASI BİYOTIP VE GENOM ENSTİTÜSÜ, MOLEKÜLER BİYOLOJİ VE GENETİK (DR) (İNGİLİZCE)

30 September 2020 - Now (2 Year 11 Month)
Yüksek Lisans, Tezli Program, DOKUZ EYLÜL ÜNİVERSİTESİ, TÜRKİYE
İZMİR ULUSLARARASI BİYOTIP VE GENOM ENSTİTÜSÜ, MOLEKÜLER BİYOLOJİ VE GENETİK (YL) (TEZLİ) (İNGİLİZCE)
Cumulative Grade Point Average: 3.57 / 4.0

03 September 2014 - 29 July 2020 (5 Year 11 Month)
Lisans, Anadal/Normal Öğretim, ORTA DOĞU TEKNİK ÜNİVERSİTESİ, TÜRKİYE
FEN-EDEBİYAT FAKÜLTESİ, MOLEKÜLER BİYOLOJİ VE GENETİK PR. (İNGİLİZCE)
Diploma Number: 143353
Cumulative Grade Point Average: 2.29 / 4.0

Foreign Language Information

İNGİLİZCE (Reading: İyi, Writing: İyi, Speaking: İyi)

TÜBİTAK Scholarships and Fundings

Project Info	120C129, Nöroendokrin ve Nöroendokrin-Benzeri Mesane Tümörlerinde ß-cateninin Rolü, Burslu, Yürürlükte, BİDEB - Eğitim Burs Ve Etkinlik Destekleri Grubu, BİDEB-2247A / Genç Araştırmacı, BİDEB, Project Participation/Leave Dates: 12/1/22 - Devam ediyor, Project Start/End Dates: 4/1/21 - 4/1/24. 120S945, Sıklıkla Delesyona Uğrayan 8p23.1 Lokusunda Yer Alan SOX7 Transkripsiyon Faktörünün Multipl Miyelom Gelişimi ve Tedavi Direncindeki Rolünün Moleküler, Epigenomik, ve Transkriptomik Yöntemlerle Karakterizasyonu, Burslu, Yürürlükte, SBAG - Sağlık Bilimleri Araştırma Destek Grubu, 1001 - Araştırma, ARDEB, Project Participation/Leave Dates: 11/1/21 - 1/3/22, Project Start/End Dates: 2/15/21 - 2/15/24. 118S505, Pediatrik Burkitt Lenfoma Hastalarında Dolaşımsal Serbest ve Ekzozomal MikroRNA İfade Seviyelerinin İnvazif Olmayan Tanı Biyobelirteci Olma Potansiyellerinin İncelenmesi, Burslu, Sonuçlandı, SBAG - Sağlık Bilimleri Araştırma Destek Grubu, 1001 - Araştırma, ARDEB, Project Participation/Leave Dates: 2/24/21 - 11/1/21, Project Start/End Dates: 11/1/18 - 5/1/22.
BIDEB Supports	EZGİ BOYVATLI, Etkinlik Destekleri ve Eğitim Bursları Müdürlüğü, 2210-A Genel Yurt İçi Yüksek Lisans Burs Programı, Başvurusu Reddedildi, 2020 - 2, 10/1/20 - 9/30/22. EZGİ BOYVATLI, Etkinlik Destekleri ve Eğitim Bursları Müdürlüğü, 2210-A Genel Yurt İçi Yüksek Lisans Burs Programı, Başvurusu Reddedildi, 2021 - 2, 10/1/21 - 9/30/23.

Number of Panelist/Observer/Reporter Jobs

Refereeing/Panelist/Outer Consultant Count	ARDEB/BİDEB 0	TEYDEB 0	Total 0
Number of Observer/Consultant Jobs	ARDEB/BİDEB 0	TEYDEB 0	Total 0
Number of Reporter Jobs	ARDEB/BİDEB 0	TEYDEB 0	Total 0